POLITECNICO DI TORINO
Repository ISTITUZIONALE

Feasibility analysis of integrating solar thermal technologies into district heating network with urban building energy modeling

*Original*
Feasibility analysis of integrating solar thermal technologies into district heating network with urban building energy modeling / Usta, Y., Montazeri, A., Mutani, G.. - In: ENERGY AND BUILDINGS. - ISSN 0378-7788. - 338:115661(2025). [10.1016/j.enbuild.2025.115661]

*Availability:*
This version is available at: 11583/2998684 since: 2025-04-14T09:12:35Z

*Publisher:*
Elsevier

*Published*
DOI:10.1016/j.enbuild.2025.115661

*Terms of use:*

This article is made available under terms and conditions as specified in the corresponding bibliographic description in the repository

*Publisher copyright*

(Article begins on next page)

06 September 2026

Energy & Buildings 338 (2025) 115661

Contents lists available at ScienceDirect

Energy & Buildings

journal homepage: www.elsevier.com/locate/enb

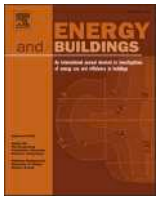

# Feasibility analysis of integrating solar thermal technologies into district heating network with urban building energy modeling☆

Y. Usta, A. Montazeri, G. Mutani *

*Department of Energy Politecnico di Torino, Italy*

ARTICLE INFO

*Keywords:*
Urban building energy modeling
Solar thermal collectors
Photovoltaics
District heating
Geographic information system
Self-consumption
Self-sufficiency

ABSTRACT

The aim of this work is to study the effects of utilizing cleaner technologies in district heating networks and assess their contribution to the energy transition within densely populated urban areas. In this context, this study presents a methodology using Urban Building Energy Modeling (UBEM) with a place-based approach to assess the potential of integrating solar thermal collectors for space heating and hot water production services. Moreover, it compares their feasibility with photovoltaic panels. The proposed methodology can be applied to various urban contexts with different climate conditions using an open-source tool and available databases. The methodology adopts a bottom-up approach with a building as the territorial unit, and it takes into account site specific climate condition, building characteristics, urban features, and local constraints. The key step presented in this work is a detailed roof segmentation method used to evaluate the available areas on different roof orientations. The results show an increase in self-consumption and self-sufficiency levels when solar production is utilized for multiple energy services compared to a single service. This increase is three-fold in self-consumption index when hot water is added to the space heating service (a rise from 10% to 31%), and double for self-efficiency index, that is, from 12 to 24%. By using energetic, economic and social indicators, this study contributes to defining target indicators and indexes, while considering local constrains, to achieve the overarching goal of sustainability in energy system. This is aligned with the efforts that are being made to create sustainable cities through collective actions.

## 1. Introduction

The increasing demand for energy, which is driven by rapid urbanization and industrial growth, presents a major challenge in reducing energy-related carbon emissions. By 2018, urbanization in the European Union (EU) had reached 74.5 % and it is expected to reach 83.7 % by 2050, highlighting the need to mitigate the increasing energy demand in densely populated urban areas. In this context, integrating renewable energy technologies into urban environments and transitioning to sustainable energy sources have become crucial strategies to respond to climate change concerns [1].

Following the implementation of ambitious targets and agreements, the share of renewables in the EU increased from 12.5 % in 2010 to 23 % in 2022 [2]. However, despite policies and targets outlined in documents, such as the Paris Agreement [3] and the concept of a Circular Economy [4], fossil fuels still dominate the global energy mix, accounting for 70 % of the EU's gross available energy [5]. This reliance highlights the urgent need for innovative solutions to decarbonize energy systems, particularly for thermal energy. Within this framework, cities – due to their diverse end-use sectors – present significant opportunities to address this challenge and to integrate more renewable energy [6].

Among possible technologies, solar collectors/panels have emerged as a promising solution due to their installation flexibility, even in dense urban settings. The photovoltaic market is growing fast, with a compound annual growth rate of 25.88 % by 2032. Meanwhile, the global solar thermal market grew by 3 % in 2021, becoming the third-largest energy supplier after wind power and photovoltaics [7]. Italy experienced a remarkable annual growth of 83 % in 2021, sustaining momentum with a 43 % increase in 2022.

The building and industrial sectors currently consume about 97 % of their final energy for heat; 53 % from industrial processes, while 44 % is used in buildings for space heating and hot water [8]. The heating sector remains heavily dominated by fossil fuels, with only 11 % of global heating needs met by renewables in 2021. The contribution of

☆ This article is part of a special issue entitled: 'Sustainable energy communities' published in Energy & Buildings.

* Corresponding author.
*E-mail addresses:* yasemin.usta@polito.it (Y. Usta), ahad.montazeri@polito.it (A. Montazeri), guglielmina.mutani@polito.it (G. Mutani).

https://doi.org/10.1016/j.enbuild.2025.115661
Received 30 November 2024; Received in revised form 24 February 2025; Accepted 24 March 2025
Available online 25 March 2025
0378-7788/© 2025 The Author(s). Published by Elsevier B.V. This is an open access article under the CC BY license (http://creativecommons.org/licenses/by/4.0/).

**Nomenclature**

| | |
|---|---|
| C | Consumption, kWh |
| CAP | Postal Code (Codice di Avviamento Postale, in Italian) |
| CDD | Cooling Degree Days, °C |
| DHN | District Heating Network |
| DHW | Domestic Hot Water |
| DSM | Digital Surface Model |
| DTM | Digital Elevation Model |
| E | Electrical energy |
| $E_h$ | Exergy, kWh |
| EP | Energy Poverty |
| EPI | Energy Poverty Index, % |
| H | Space Heating |
| HDD | Heating Degree Days, °C |
| LGBM | Light Gradient Boosting Machine |
| ML | Machine Learning |
| NDVI | Normalized Difference Vegetation Index, [-] |
| OPI | Over Production Index, % |
| P | Production, kWh |
| PR | Performance Ratio, % |
| $Q_h - Q_e$ | Energy Production, kWh |
| RES | Renewable Energy Source |
| RMSE | Root Mean Square Error |
| SC | Self-consumption, kWh |
| SCI | Self-consumption Index, % |
| SSI | Self-sufficiency Index, % |
| STC | Solar thermal collectors |
| T | Temperature, K |
| $T_L$ | Linke turbidity factor |
| UBEM | Urban Building Energy Modeling |

renewables to space heating and cooling reached 22.9 % in Europe in 2021 [5], which is twice the global share, but this production still does not cover even a quarter of total heat consumption.

Given that heating accounts for most of the final energy consumption across all the different sectors, solar thermal energy holds great potential, not only in providing hot water and space heating but also as a sustainable solution for district heating networks (DHNs) in urban areas [9]. The scalability of solar thermal for urban district heating (DH) systems could be a cost-effective path to achieve carbon–neutral DH systems, aligning with climate targets set by the member states. The "Net Zero Emissions by 2050 Scenario" [10] presents a promising strategy by the member states, as it combines clean energy technologies with energy efficiency measures.

Despite remaining stable in 2022, DH systems continue to supply around 9 % of the global final heating demand for buildings and industry [11]. However, since DH is responsible for nearly 4 % of global $CO_2$ emissions, urgent action is needed to reduce its emissions. To meet climate targets, the $CO_2$ intensity of district heat production should decrease by at least 20 % by 2030 compared to the 2022 levels. However, fossil fuels still dominate the DH supply market, with renewables composing only a small share. Some European countries, such as Sweden, Denmark, and Austria, lead in renewable integration, with over 50 % of DH systems sourced from renewables.

The building and industry sectors consume roughly equal shares of the heat generated by DH plants, thereby highlighting the crucial role of DHNs in decarbonization. Thus, fostering the integration of Renewable Energy Sources (RES) into existing DHN is essential.

Recent studies have analyzed the integration of Solar Thermal Collectors (STC) into existing DHN demonstrating their potential to meet significant portions of the total energy demand. For instance, in Latvia, which had an annual energy consumption of 51,643 and 53,220 MWh in 2019 and 2020, STC contributed by 14.7 % and 20.5 %, respectively. A further expansion of STC areas could potentially increase this contribution to 50 %, with an optimal energy storage volume of 8000 $m^3$ [12].

A recent study examined energy upgrading of a neighborhood in Yverdon-les-Bains, Switzerland [13]. It assessed the integration of new buildings with STC into a low-temperature DHN, revealing that the district was both energy flexible and self-sufficient. The results indicated that the district functioned as a Zero Energy District for 28.9 % of the year, emphasizing the importance of dynamic performance assessment in redevelopment strategies.

Another study examined solar heat injection into DHN in Switzerland, highlighting its potential as a low-carbon alternative [14]. The authors found that solar heat accounted for approximately 17.7 g $CO_{2\text{-eq}}$ per kWh of useful heat, with manufacturing components and operational energy-use being the main environmental impact factors. Sensitivity analyses showed that parameters such as lifetime, efficiency, and electricity mix significantly affect greenhouse gas (GHG) emissions. This study provided valuable insights for promoting sustainable heating solutions and suggested future research on synergies with other low-carbon energy carriers and storage solutions for intermittent solar thermal production [14].

Despite the benefits of integrating STC into existing DHN, challenges remain. Selvakkumaran et al. not only highlighted the drivers but also the barriers to integrating solar prosumers into the Swedish DH system [15], including cost, technical challenges, and policy uncertainties, thereby hindering the integration of solar heat into DH systems.

These studies have demonstrated the benefits of integrating STC into DHN and underscored the crucial role of the building sector in decarbonizing the existing energy supply systems in cities. The following sections will present a flexible methodology for analyzing STC production at different temperatures to meet the energy demand using the local DHN. Additionally, a feasibility study is conducted to compare STC with PV technologies, presenting the energetic, economic, and social impacts.

## 2. Knowledge gap and the objective of the work

This work focuses on integrating STC into existing DHNs to advance renewable energy use in dense urban environments and optimize existing energy systems. There is a need for urban-scale assessment methodology that accounts for the site-specific characteristics of the built environment – including physical, regulatory, and legal constraints that can limit the installation of solar technologies. In this context, the work employs a data-driven Urban Building Energy Modeling (UBEM) approach [16] to analyze integration scenarios of STC in the DHN of Turin (Italy) and compare these scenarios with those of PV systems.

The contributions of this work can be defined as follows:

- Urban-scale roof assessment: a detailed roof segmentation analysis is introduced to calculate the net roof area for each different roof orientation, excluding the constraints. This allows the analysis and comparison of the potential production from each roof orientation.
- Maximizing self-consumption: the work presents several scenarios to identify the most effective strategies for maximizing self-consumption (SC) from STC and PV technologies.
- Economic and social feasibility: besides the energetic indexes, the work examines the economic and social implications of integrating solar technologies into existing energy systems.

Overall, this research addresses a critical gap in understanding how detailed analysis of solar technologies can be effectively deployed in

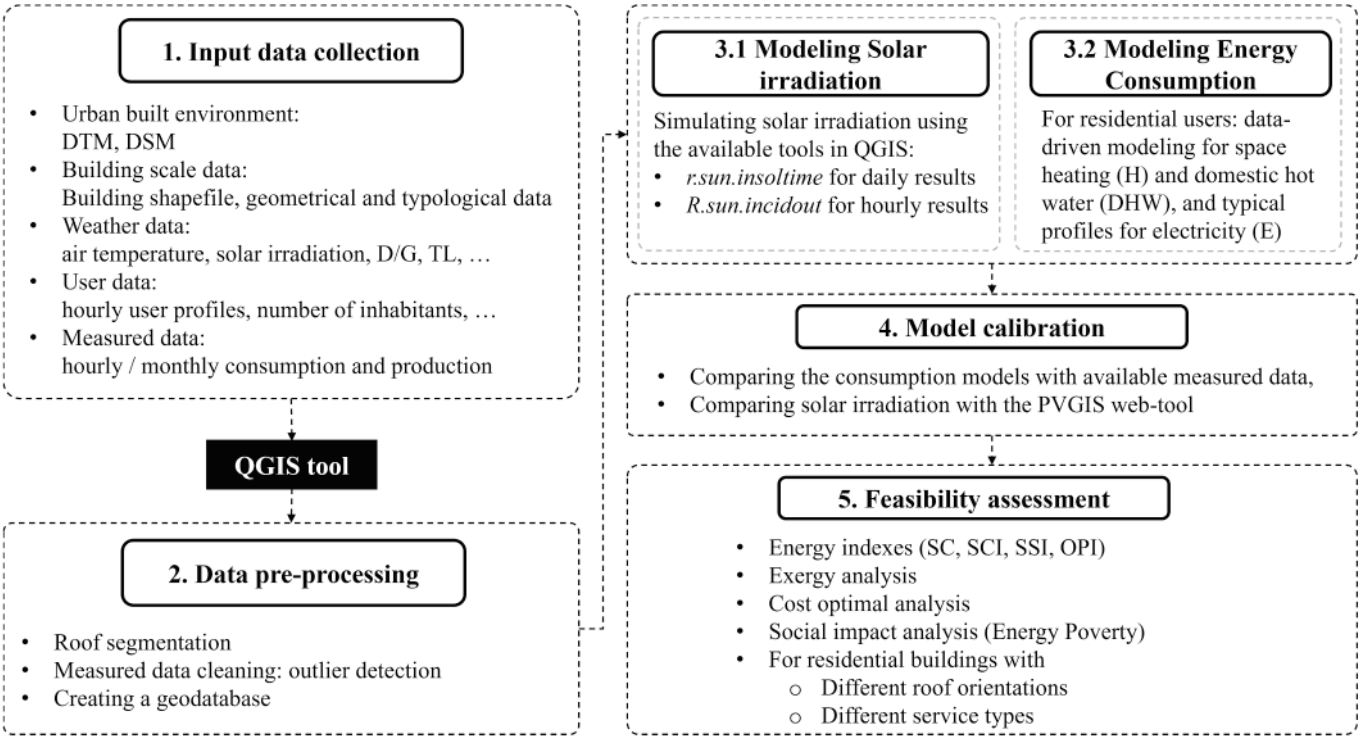


**Fig. 1.** The general methodology for QGIS-based STC and PV analysis.

urban settings to achieve sustainability goals, reduce dependency on fossil fuels, and integrate more RES into existing energy systems [17]. This evaluation aligns with the European Union's decarbonization objectives and provides insights relevant to various urban contexts.

## 3. Materials and methods

This work has used a place-based methodology to analyze the solar energy potential in Turin by simulating solar irradiation on all building rooftops using the open-source tool QGIS (Quantum Geographic Information System, version 3.34). QGIS is a GIS platform that supports spatial analysis, data visualization, and geospatial modeling. For solar irradiation calculations, QGIS integrates advanced plugins, which uses 3D models of the built environment to simulate solar exposure and shadowing effects. This capability allows for accurate estimation of solar potential across urban landscapes. The general methodology for QGIS-based solar technology analysis is presented in Fig. 1.

The first step is data collection, which shows that this methodology can be adapted to different urban contexts; using diverse input data, which may vary across different spatial and temporal scales. Since a 3D representation of the built environment is needed for the irradiation simulation, a Digital Surface Model (DSM) was used in this work. However, if this input data is not available, alternatives, such as 2D building footprints extruded by their heights, can be employed. This approach ensures flexibility of the method across diverse datasets and emphasizes the impact of the accuracy of input data on the final outcomes.

Step 2 is the most critical step in this methodology, as it involves creating a geo-database from the pre-processed input data, which forms the core of the model. This step includes two main analyses:

- Segmenting building roofs, assigning each segment its orientation and slope, and calculating the available roof area for panel installation while accounting for physical, cultural, historical, and legal constraints,
- Pre-processing and cleaning measured consumption data, georeferencing them to be associated with the building layer. This step is essential to train the ML model to predict energy consumption for all residential buildings in Turin.

The accuracy of the analyses in this step is essential for the final evaluation of solar technology potential. Therefore, extensive processing and testing are conducted to ensure a high quality of the geodatabases used in the subsequent steps.

Step 3 applies the modeling of the energy production and consumption for all residential buildings. In this work, solar irradiation simulations consider the real sun and sky conditions and the morphology of the city of Turin, with the different monthly and daily variations.

For energy consumption modeling, a data-driven model is used to evaluate the space heating and domestic hot water consumption. While for electricity consumption, typical monthly profiles of residential users were applied to each dwelling.

Step 4 is the model validation. The results of the space heating and domestic hot water consumption modeling was compared against real measured data. The solar simulations were validated by comparing their results with PVGIS; a free web application for solar radiation and PV analysis. The validated models ensure that the energy consumption and production of the buildings would be correctly used in testing future RES integration scenarios.

Step 5 associates the energy consumption with production data to evaluate various sustainability indicators and indexes. Considering different scenarios, it was possible to analyze: PV and STC productions, self-consumption and self-sufficiency indexes, energy and investment costs, and energy poverty.

## 4. Input data

This section provides the input data used in QGIS for this work. At this point, it is important to stress the importance of input data precision for model reliability.

**Table 1**
Typical days, average solar irradiation ($H_{day,avg}$) and input data for the solar characteristics over the different months.

| | Jan | Feb | Mar | Apr | May | Jun | Jul | Aug | Sep | Oct | Nov | Dec |
|---|---|---|---|---|---|---|---|---|---|---|---|---|
| Typical day | 17 | 16 | 16 | 15 | 15 | 11 | 17 | 16 | 15 | 15 | 14 | 10 |
| $H_{day,avg}$ [kWh/m$^2$] | 1.75 | 2.56 | 3.90 | 4.92 | 5.74 | 6.45 | 6.60 | 5.78 | 4.45 | 2.75 | 1.69 | 1.41 |
| D/G [-] | 0.43 | 0.42 | 0.39 | 0.41 | 0.42 | 0.39 | 0.36 | 0.37 | 0.39 | 0.46 | 0.50 | 0.47 |
| $T_L$ [-] | 2.58 | 2.79 | 3.26 | 3.77 | 3.74 | 3.76 | 3.51 | 3.43 | 3.34 | 3.25 | 2.84 | 2.55 |

*Urban built environment.* A Digital Surface Model (DSM), with 1 m precision, was used for the 3D representation of the city of Turin. This precision provides a good balance between simulation cost and result accuracy considering urban scale analysis [18,19]. However, a Digital Terrian Model (DTM) or extruded building footprints (the height of the buildings being known) can also be used as alternative data for the urban environment representation in case a DSM is not available.

*Building data.* The building characteristics were downloaded from the BDTRE (Base Dati Territoriale di Riferimento degli Enti piemontesi), the geoportal database of the Piedmont Region related to the year 2023 [20]. A total of 44,289 buildings (and building blocks) were available for the city of Turin, with 53 % having been categorized as only residential buildings. Additionally, the cultural and historical constraints (art. 10 D. Lgs 42/2004) were downloaded from the regional geoportal [21].

*Solar radiation parameters.* The used weather data as an input for the solar irradiation simulations were the average monthly values of diffuse-to-global solar irradiation (D/G) for 2006–2020 [22]. Another weather-related data were the monthly average Linke turbidity factors ($T_L$) obtained from Meteonorm (version 8.0) [23]. D/G is an important parameter in understanding the scattering ratio of solar radiation, and it can vary according to the atmospheric conditions, such as cloud cover. Similarly, $T_L$ was used to evaluate the state of the solar radiation transmittance of the atmosphere in a specific location. Both parameters are fundamental in solar assessment for the irradiation simulation in the QGIS environment. Table 1 provides the monthly values of both parameters, together with the average solar irradiation for a typical day in each month, selected based on the work of Duffie & Beckman, 1991 [24].

*Residential users.* The number of inhabitants and families in each building were calculated using the population data of the census sections from the Italian National Institute of Statistics (ISTAT) [25].

*Energy consumption data.* The available measured data covered the typical consumption of residential families in Turin. The space heating and domestic hot water consumption data were taken from those recorded by the local DH company during the 2022–2023 period. The typical electrical energy consumption (E) of residential users was derived from ARERA [26].

## 5. Data pre-processing

The input data provided in the previous section were pre-processed to assign them to the residential buildings used in this work. This step

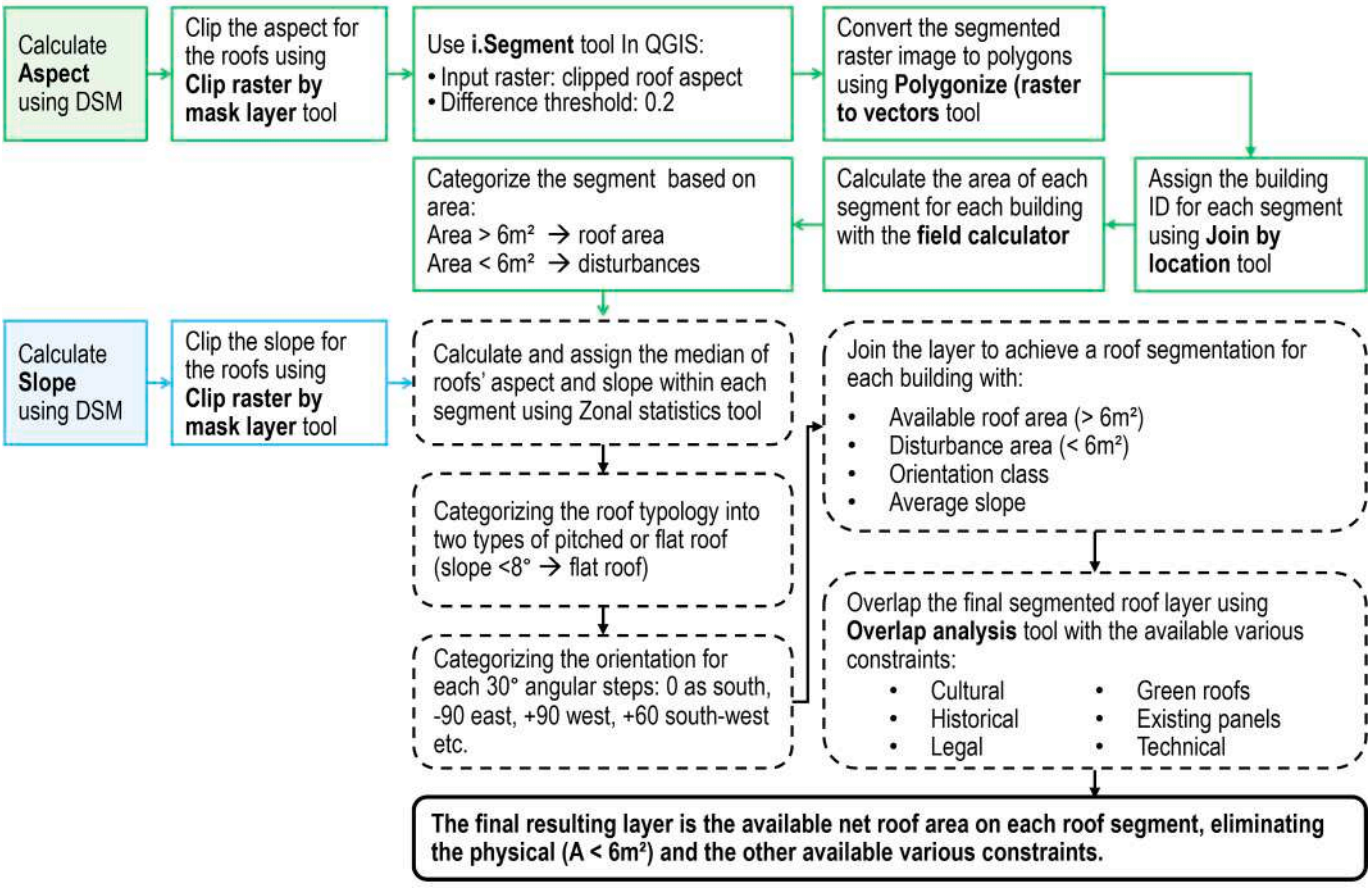


**Fig. 2.** Roof segmentation steps used in QGIS to obtain 13 roof orientation categories with the median slope of each orientation (steps in green boxes use aspect layer, blue boxes use slope layer, and black boxes represent the joined layers).

ensured compatibility of the results from the analysis performed within the QGIS environment, which were used to model the energy consumption and production of the buildings in Turin.

*Built environment and building data.* The DSM was used in QGIS to obtain a 3D city model and in particular the slope and aspect of building roofs, which was possible using *Raster terrain analysis* tool. The aspect is defined by the solar azimuth: South equals 0°, East −90°, and West +90°, while the slope is expressed in degrees. The aspect and slope raster images were used to categorize areas with similar roof segmentation characteristics.

The building shapefile was also used to calculate the area, the volume, and the number of inhabitants per building, which were needed and used for the energy consumption modeling.

*Roof segmentation.* As mentioned earlier, this study presents a detailed description of a roof segmentation method implemented with QGIS. This method significantly enhances the evaluation of STC and PV potential by quantifying the net available roof area for diverse roof orientations. The method has been applied to all buildings in Turin, defining 13 roof categories; 12 categories of roof orientation for inclined roofs, using 30° angular steps (with south 0°, east −90°, west 90°) plus one category for flat roofs. Fig. 2 provides the steps followed in QGIS for roof segmentation.

This method uses *i.segment* tool in QGIS to identify building roof segments using the aspect raster file. Converting the aspect raster file to vector file, using *Polygonize* tool, allows to dissolve the aspect pixels having similar values into one roof segment; thus, each building will have several roof segments based on its roof type. These segments were then assigned median slope and aspect values to enable roof categorization: the slope is used to define the roof type by inclination, with slope less than 8° considered flat, and for inclined roofs, the aspect is used to determine their orientation in 30° intervals. Moreover, checking the area of each dissolved roof segment allowed to evaluate if the segment is either a physical constraint like chimney, dormers, etc, or a useful area for solar panel installation. The threshold of the area for physical constraints is set to 6 $m^2$.

Finally, the shapefile related to the cultural, historical, and legal constraints were overlapped with the final segmented roof shapefile to analyze the available roof areas by excluding these constraints. This step was performed using the *overlap analysis tool* in QGIS to calculate the net area available for roof-integrated solar technologies.

However, it is important to note that existing solar panels and the green roofs are not among the constraints considered in this work. Considering the green roofs, an overlap analysis of the flat roofs with the Normalized Difference Vegetation Index (NDVI) raster is conducted using raster image extracted from Google Earth Engine with the precision of 30 m × 30 m. The resulting overlap percentage of 0.5 shows that the share of the green roofs over the total available roof area is minimal in the city of Turin. However, this percentage is still not reliable due to the precision of the available NDVI raster which is overestimating the green roofs. Identifying these elements (green roofs and existing panels) requires advanced image detection techniques [27] using high-resolution orthophotos, which is not feasible for large-scale assessments, such as the city-scale analysis conducted in this study.

*Solar radiation parameters.* The solar radiation parameters were required as raster images to be used in the QGIS simulations. Thus, monthly D/G and $T_L$ data were utilized to generate a total of 24 raster images: 12 D/G and 12 $T_L$. This conversion process was conducted with the *raster calculator* tool.

*Residential users.* The number of inhabitants in each single building was calculated as a function of the buildings' volume within census sections, using equation (1). The open-source demographic data are available in census section scale which is the aggregated information of the buildings within each census. To down-scale the data, building volumes are used to assign these demographic data to each single building [28].

$$N_{families,b} = \frac{N_{families,cs} \cdot V_{building}}{\sum V_{building}} \quad (1)$$

where:

$N_{families,b}$ is the number of families in each building.

$N_{families,cs}$ is the number of families in each census section.

$V_{building}$ is the volume of each building.

$\sum V_{building}$ is the sum of building volumes in the census section.

*Energy consumption data.* Data from 6095 substations and the relative consumptions by type of service were georeferenced and associated with the buildings in Turin. The energy data were then subdivided by service typology: 3943 with heating service for 7 months (H), 374 for heating and domestic hot water service (H + DHW), and 3 buildings for DHW service.

## 6. Solar irradiation simulation and energy production model

Simulations of the daily solar irradiation were performed in QGIS with the *r.sun.insoltime* tool. This tool utilizes DSM, aspect, and slope raster images as input data to represent the built environment. The *r.sun.insoltime* tool uses the monthly values of D/G, $T_L$, and the albedo for solar radiation to determine the atmospheric and urban conditions in solar analysis.

Once the solar irradiation was known, the energy produced by STC was calculated:

$$Q_h = A_c \cdot H_{sol} \cdot \eta_{STC} [\text{kWh}] \quad (2)$$

where:

$Q_h$ is the thermal energy production [kWh].

$A_c$ is the net area of the collector [$m^2$].

$H_{sol}$ is the incident solar irradiation [kWh/$m^2$].

$\eta_{STC}$ is the thermal collector efficiency [-].

The efficiency of the solar thermal collectors was calculated considering the local climate conditions and the characteristics of the panels:

$$\eta_{STC} = \eta_0 - a_1 \cdot \frac{\Delta T_m}{I} - a_2 \cdot I \cdot \left(\frac{\Delta T_m}{I}\right)^2 [-] \quad (3)$$

where:

$\eta_0$ is the optical efficiency of the solar collector.

$a_1$ is the linear heat loss coefficient [W/($m^2$K)].

**Table 2**
The monthly performance ratio of the PV panels for each roof orientation.

| Orientation | Jan | Feb | Mar | Apr | May | Jun | Jul | Aug | Sep | Oct | Nov | Dec |
|---|---|---|---|---|---|---|---|---|---|---|---|---|
| **−90°** | 0.837 | 0.846 | 0.840 | 0.820 | 0.803 | 0.785 | 0.776 | 0.780 | 0.800 | 0.823 | 0.815 | 0.817 |
| **−60°** | 0.868 | 0.858 | 0.840 | 0.817 | 0.801 | 0.782 | 0.772 | 0.778 | 0.799 | 0.831 | 0.841 | 0.858 |
| **−30°** | 0.878 | 0.861 | 0.838 | 0.814 | 0.798 | 0.781 | 0.771 | 0.775 | 0.797 | 0.832 | 0.851 | 0.872 |
| **0°** | 0.882 | 0.862 | 0.838 | 0.812 | 0.797 | 0.779 | 0.768 | 0.773 | 0.796 | 0.833 | 0.856 | 0.879 |
| **30°** | 0.876 | 0.859 | 0.837 | 0.814 | 0.796 | 0.778 | 0.768 | 0.774 | 0.796 | 0.831 | 0.852 | 0.874 |
| **60°** | 0.866 | 0.856 | 0.836 | 0.814 | 0.797 | 0.778 | 0.768 | 0.774 | 0.796 | 0.829 | 0.842 | 0.861 |
| **90°** | 0.835 | 0.844 | 0.835 | 0.815 | 0.798 | 0.779 | 0.770 | 0.775 | 0.794 | 0.821 | 0.819 | 0.821 |
| **Flat** | 0.809 | 0.835 | 0.838 | 0.821 | 0.804 | 0.786 | 0.777 | 0.782 | 0.800 | 0.820 | 0.801 | 0.785 |

$\Delta T_m$ is the mean panel temperature, which is the average of the inlet and outlet water temperatures [K].

$I$ Is the solar irradiance [W/m$^2$].

$a_2$is the non-linear heat loss coefficient [W/(m$^2$K$^2$)].

The same methodology was used to calculate the production of electricity:

$$Q_e = PR \cdot H_{sol} \cdot S \cdot \eta_{PV} \text{ [kWh]} \quad (4)$$

where:

$Q_e$ is the electrical energy production [kWh].

PR is the performance ratio of the system [%].

$H_{sol}$ is the incident solar irradiation [kWh/m$^2$].

S is the active surface of the panel [m$^2$].

$\eta_{PV}$ is the conversion efficiency of the PV panels [−].

The performance ratio (PR) was calculated on monthly basis taking into account the different performances of the PV compared to the standard test conditions, at temperature of 25 °C and solar irradiance of 1000 W/m$^2$ [29].

Table 2 reports the monthly values of the performance ratio calculated for the city of Turin which were used to calculate the electricity that can be produced on each roof orientation. In general, the PR is higher in winter when outdoor temperature is lower and for south oriented roofs (indicated with 0°).

## 7. Energy consumption modeling

A data-driven model that incorporated a Machine Learning (ML) algorithm was utilized to predict the space heating and domestic hot water consumption of the residential buildings in Turin. A Light Gradient Boosting Machine (LGBM) was selected to predict the end-user energy consumption. LGBM is a Machine Learning algorithm that is based on decision trees. It creates trees sequentially, and it corrects the errors of previous trees at each level. LGBM is based on leaf-wise growth, which leads to fast convergence; thus, this model is fast in regression tasks. The ML algorithm was appropriately tuned to model the energy consumption by tuning its essential hyperparameters, using the benefits of the Optuna optimizer machine and the cross-validation technique. The data obtained from the DH company allowed the model to be trained and tested for space heating (H) and domestic hot water (DHW).

The electrical energy consumption (E) of each family was calculated using the average monthly energy consumption per residential user [25] and the number of families in each building in the city of Turin [26].

## 8. Self-consumption and self-sufficiency scenarios

Nine scenarios were investigated considering the use of STC, operating at different inlet–outlet temperatures [30], the use of PV panels for three different energy services (i.e., H, DHW and E), and considering both the buildings connected to and those not connected to the DHN.

The simulated scenarios for the buildings connected to the DHN were:

- Scenario 1: STC at 60 – 105 °C for H service
- Scenario 2: STC at 50 – 90 °C for H service
- Scenario 3: STC at 60 – 70 °C for H service
- Scenario 4: STC at 50 – 60 °C for H service
- Scenario 5: STC at 40 – 50 °C for H service
- Scenario 6: STC at 40 – 50 °C for H + DHW services

The simulated scenarios for the buildings not connected to the DHN were:

- Scenario 7: STC at 15.3 – 80 °C for H service
- Scenario 8: STC at 15.3 – 40 °C for DHW service.

Finally, the scenario for the electricity service was:

- Scenario 9: PV panels for electricity (E) service.

The inlet temperature of 15.3 °C adopted in Scenarios 7 and 8 represents the average outdoor air temperature recorded in Turin during the 2022–23 heating period. These two scenarios simulated autonomous energy systems for H and DHW services that were not connected to the DHN.

The inlet–outlet water temperatures were considered important to evaluate the efficiency of the STC required for the calculation of the energy production in all the scenarios. The incident solar irradiation data was used to calculate the energy production for STC and PV for each roof in the city of Turin considering the relative available net area.

The resulting energy production was then used to assess the energy self-consumption (SC) of each building on daily time step. Self-consumption is the amount of energy that is self-consumed by a building from its RES production. Later the self-consumption and self-sufficiency indexes (SCI and SSI) were calculated on daily, monthly, and annual timeframes. SCI is the self-consumed energy of a building to its overall RES production, while SSI is the self-consumed energy of a building to its overall consumption. The former indicates the share of RES integration in a building, while the latter defines how much the building is energy independent.

Moreover, by aggregating buildings' energy consumption and production at different scales, it was possible to evaluate the quantity of shared energy and the collective self-consumption [31]. This indicator is useful to measure how the over-production of energy, which can be used by other users or members of a community, can be exploited instead of being fed into the grid.

The consumption (C) and production (P) being known, Eq. (5.1) and Eq. (5.2) were used to calculate the energy indicator and indexes.

$$\begin{aligned}
&\text{Self-Consumption} \quad SC = minimum(C, P) \\
&\text{Uncovered Demand} \quad (C - P)\ if\ (C - P) \geq 0 \quad (5.1) \\
&\text{Over-Production} \quad (P - C)\ if\ (P - C) \geq 0
\end{aligned}$$

$$\begin{aligned}
&\text{Self-consumption Index} \quad SCI = \frac{SC}{P} \\
&\text{Self-sufficiency Index} \quad SSI = \frac{SC}{C} \quad (5.2) \\
&\text{Over-Production Index} \quad OPI = \frac{OP}{P} \\
&\text{Energy Poverty Index} \quad EPI = \frac{Energycosts}{Income}
\end{aligned}$$

## 9. Exergy analysis

The energy analysis provided previously presented the calculation of energy produced by solar collectors at different temperatures. However, energy analysis alone does not indicate how effectively that energy can be converted into work. To address this, exergy analysis was also evaluated to take into account the quality of the energy produced at different temperatures. Exergy measures the maximum useful work that can be produced with a theoretical system from a given quantity of thermal energy at a certain temperature. In literature, the analysis of solar collectors considers the exergy content of the water flow, pertaining to its temperatures, using factors such as the Carnot factor or the Gouy-Stodola Theorem [32]. This approach provides a more comprehensive understanding of the system performance by not only measuring the total energy produced but also assessing its potential to perform useful

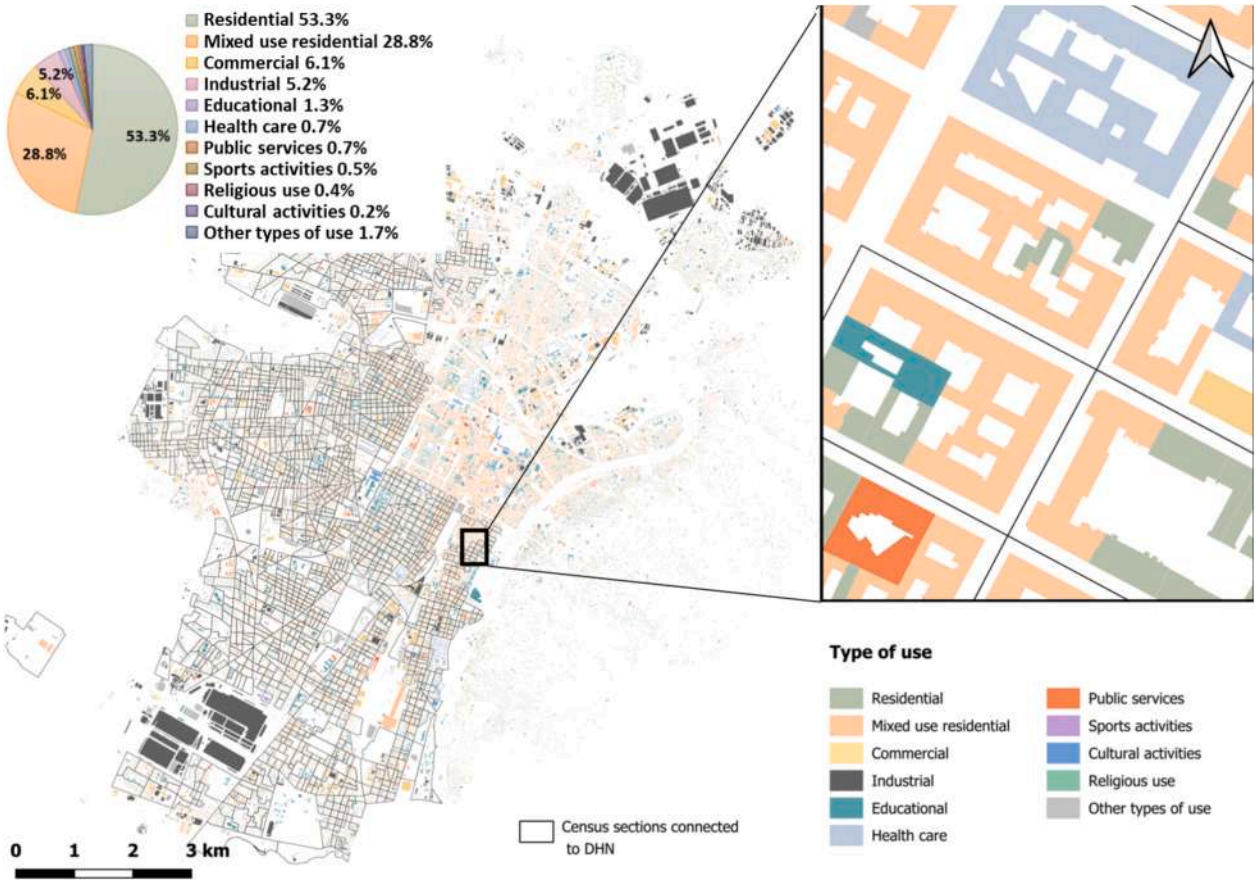


**Fig. 3.** The city of Turin with the DHN area and the different building typologies.

work. Consequently, the energetic indexes for both energy and exergy can be calculated, enabling a direct comparison.

The exergy content of a thermal collector can be measured with:

$$E_h = Q_h \cdot \left(1 - \frac{T_0}{T_{out}}\right) \text{[kWh]} \quad (6)$$

where:

$Q_h$ is the energy produced by STC [kWh].

$\left(1 - \frac{T_0}{T_{out}}\right)$ is the Carnot factor [-].

$T_0$ is the reference temperature of the *dead state,* which is used to describe the zero-exergy condition; this temperature is 293.15 or 298.15 in the literature for annual analyses or the minimum outside air temperature recorded over a month in monthly analyses [K].

$T_{out}$ is the outlet temperature of the STC [K].

When energy is measured with the Carnot factor, it is measured from the dead state of $T_0$ to the outlet temperature. When exergy is measured with the Gouy-Stodola Theorem, the exergy content depends on the temperature gradient between the inlet and outlet water, and the exergy can be obtained by substituting $T_{out}$ in Eq. 6 with the Mean Thermodynamic Temperature $T_m$:

$$T_m = \frac{T_{out} - T_{in}}{ln(T_{out}/T_{in})} \text{[K]} \quad (7)$$

## 10. Socio-economic analysis

The global cost of the different scenarios was calculated to evaluate their economic convenience. The global cost was calculated using Eq. 8 [33] and was normalized for each household considering the number of families residing in each residential building:

$$C_G(t) = C_I + \sum_j \left[ \sum_{i=1}^{t} \left(C_{a,i}(j) \times R_d(i)\right) - V_{f,i}(j) \right] [€] \quad (8)$$

where:

$C_I$ is the initial investment cost [€].

$C_{a,i}$ is the annual cost for year *i*, related to the component j (operation and management costs, running costs, substitution costs) [€].

$R_d(i)$ is the discount factor for year *i* [%] (i.e., 3 %).

$V_{f,i}(j)$ is the residual value of the component j at time i, [€].

The assumptions on the investment cost for the installation of solar panels and the energy costs for various services in Italy are reported hereafter.

Cost of solar technologies:

- Flat-plate solar collector: 800 €/$m^2$
- Vacuum tube solar collector: 1200 €/$m^2$
- Photovoltaic panel (according to the c PV capacity class, PVc): 1000 €/kW if PVc > 20 $kW_p$; 1600 €/kW if 6 $kW_p \leq$ PVc $\leq$ 20 $kW_p$ and 2000 €/$kW_p$ if PVc < 6 $kW_p$.

Cost of energy:

- Thermal energy cost: Natural Gas 0.133 €/kWh and District Heating 0.10 €/kWh
- Electrical energy cost: withdrawn from the network: 0.252 €/kWh
- Electrical energy revenues: injected into the network for Northern Italy: 0.101 €/kWh.

Energy poverty (EP) was evaluated considering the average annual income of the households in the city of Turin to evaluate the social

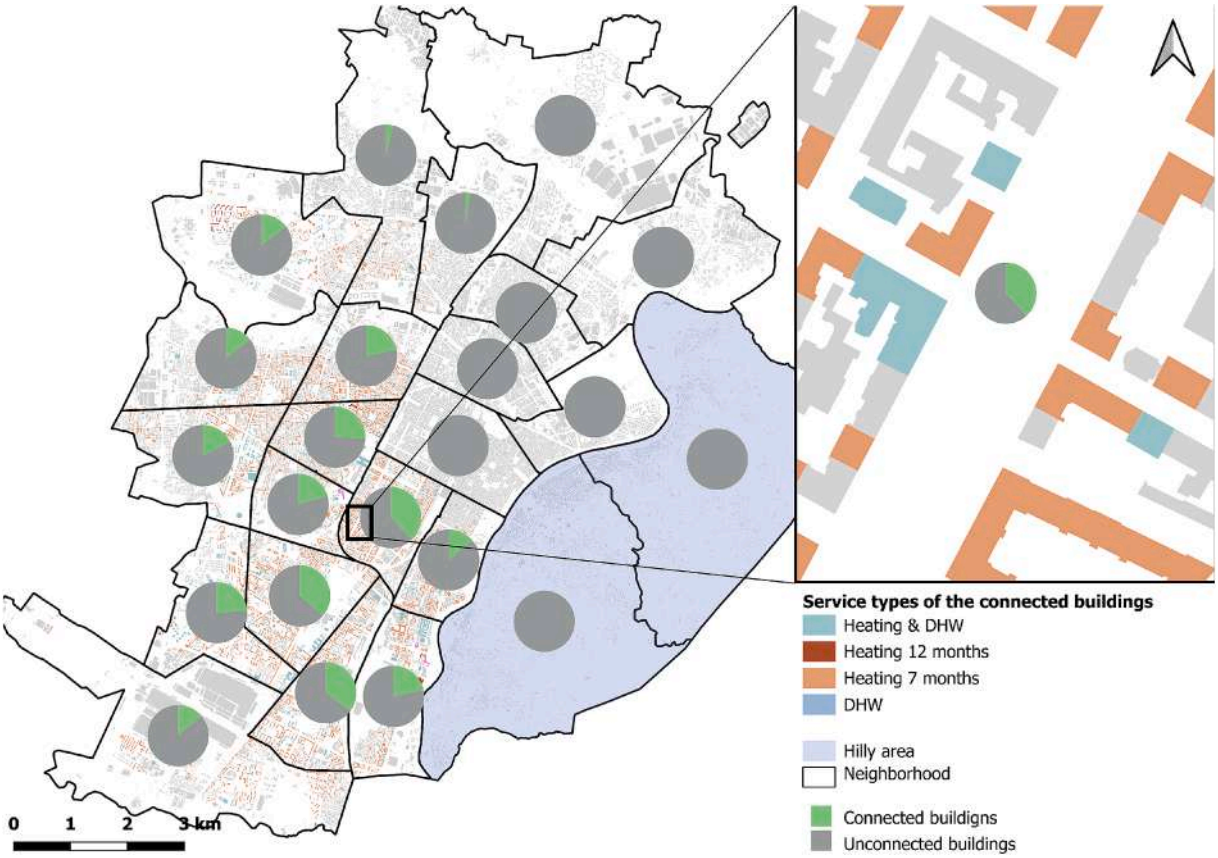


**Fig. 4.** The city of Turin with the quota of connected buildings by neighborhood (in pie charts) and the type of energy service.

impact of the use of solar technologies [34]; this information is available for each Postal Code zone. Many different indicators can be used to evaluate EP; in this work, the percentage of energy cost on the income over 10 % was considered. The scenarios also took into account incentives for low-income families, according to the Social Bonus Bills, 2024 (Bonus Sociale Bollette, 2024) [35].

## 11. Case study

Turin, which is located in the Piedmont region in Italy, hosts the largest DHN in the country. The DHN covers a significant area, with a heated volume totaling 101 million cubic meters, which represents 27 % of the region's total volume [36].

Turin has a temperate climate classified as Italian climatic zone E, with 2617 HDD at 20 °C and 84 CDD at 26 °C. The setpoint temperature within DHN during the heating season has recently been decreased to 19 °C, according to Italian Decree 383 of 6/10/2022, to satisfy the new energy-saving regulations. Fig. 3 illustrates a general overview of the city with the different building typologies and the census sections that contain buildings connected to the DHN. The residential sector comprises approximately 80 % of the existing buildings. The 'mixed-use residential' term refers to buildings which also incorporate commercial, production, office, or recreational uses (usually on the first floors). The number of industrial buildings in the northern and southern parts of the city presents an encouraging opportunity for the use of solar technologies. These buildings have large roof areas, thus making them interesting prosumers for the installation of solar systems.

Fig. 4 represents the type of energy service of the connected buildings and the quota of the buildings connected to the DHN in each neighborhood, defined by black borders. Indeed, by identifying areas with higher energy demand, it would be possible to prioritize tailored retrofitting interventions on the buildings to improve the share of renewables or to reduce the heat load and the energy costs.

**Table 3**
The main roof orientations in Turin.

| | | | | 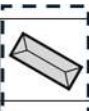 | | |
|---|---|---|---|---|---|---|
| Roof Orientation (°) | -60 | -30 | 0 | 30 | 60 | 90 |
| Number of buildings | 15,084 | 3970 | 3676 | 13,903 | 3971 | 3685 |
| (%) | 34% | 9% | 8% | 31% | 9% | 8% |

**Table 4**
Available net roof areas in Turin obtained from the roof segmentation analysis.

| | | | | | | | | | | | | | |
|---|---|---|---|---|---|---|---|---|---|---|---|---|---|
| Roof Orientation (°) | -150 | -120 | -90 | -60 | -30 | 0 | +30 | +60 | +90 | +120 | +150 | +180 | flat |
| Tot. area with disturbances (m²) | 2,740,729 | 780,624 | 1,080,154 | 2,005,562 | 781,868 | 1,105,693 | 2,808,039 | 457,636 | 1,634,045 | 3,082,150 | 897,949 | 976,010 | 3,393,589 |
| Technical disturbance (%) | 16% | 5% | 2% | 10% | 4% | 4% | 19% | 3% | 2% | 7% | 9% | 18% | 6% |
| Historical and cultural disturbances (%) | 11% | 12% | 9% | 15% | 8% | 8% | 10% | 10% | 8% | 15% | 7% | 7% | 4% |
| Tot. net area (m²) | 2,034,384 | 655,942 | 960,171 | 1,520,755 | 694,486 | 974,717 | 2,066,091 | 396,245 | 1,476,268 | 2,431,761 | 760,907 | 749,918 | 3,066,633 |
| Net area (%) | 11% | 4% | 5% | 9% | 4% | 5% | 12% | 2% | 8% | 14% | 4% | 4% | 17% |

South oriented roof area 45% of total available net area

**Table 5**
Number of buildings for the available roof area categories.

| Roof available area A | All orientations | | Good solar exposition (flat, 90° → -90°) | |
|---|---|---|---|---|
| A = 0 | 905 | *712* | 1699 | *1267* |
| 10 < A < 25 | 69 | *40* | 2494 | *1803* |
| 25 < A ≤ 60 | 3496 | *2564* | 11,834 | *9933* |
| 60 < A < 100 | 9567 | *8123* | 7611 | *6693* |
| 100 < A < 200 | 10,692 | *9212* | 6780 | *6174* |
| 200 < A < 300 | 4344 | *3927* | 1813 | *1680* |
| 300 < A < 600 | 3569 | *3362* | 1072 | *1034* |
| 600 < A < 1000 | 670 | *652* | 196 | *193* |
| 1000 < A < 5000 | 241 | *237* | 54 | *52* |

**The number of buildings, excluding the hilly area, is in gray*

**Table 6**
Number of buildings considered for the solar production analysis and their roof area.

| | N. of buildings with predicted consumption | N. of buildings with an available roof area | Available roof area [m$^2$] |
|---|---|---|---|
| All residential buildings | 33,553 | 32,198 | 3,137,727 |
| Only residential use | 20,714 | 19,781 | 1,565,647 |
| Residential with mixed use | 12,839 | 12,417 | 1,572,080 |

## 12. Results and discussion

This section provides the results of the QGIS-based solar analysis that employs a detailed roof segmentation technique to assess the potential of STC and PV technologies in future scenarios for residential buildings in Turin. The scenarios are evaluated using key energy indexes, i.e., self-consumption, self-sufficiency, and over-production indexes. Additionally, their economic and social impacts are examined by analyzing the costs of the interventions, economic savings, and the reduction in energy poverty.

## 13. Roof segmentation analysis

The roof segmentation was performed using the *i.segment* tool followed by *Polygonize* tool in QGIS to categorize building roofs. The slopes of the pitched roofs in Turin are quite constant with an average value of 29.5°. Twelve categories of roof orientation were then identified every 30°: from 0° South, to −90° East and +90° West.

Table 3 illustrates the main roof orientations in Turin, together with the number of buildings (and blocks of buildings) according to their orientation, that is, mainly −60° South − East (SE) and + 30° South − West (SW). The buildings with a South − East orientation overlook the Po River and the hilly part of the city.

Table 4 illustrates the categorization of the roofs in more detail and provides the available areas for solar technologies on each orientation considering the presence of constraints. These constraints are mainly from physical sources, e.g., the presence of dormer windows, but are also cultural, historical, and legal constraints established by local regulations and laws. For instance, the reason behind the high percentage of physical disturbances on the −60° orientation is the high presence of dormer windows for this orientation, which is mainly related to the views from the hills and along the Po River. This analysis was particularly important as it quantified the impact of constraints on the area of each roof, thereby influencing the potential energy production with solar technologies.

Table 5 provides the number of buildings by the category of available roof areas, considering all the roof orientations, the roofs with a good solar exposition from West to East (i.e., with azimuth angles from 90° to −90°), and the flat ones. It is also possible to observe the number of buildings excluding the hilly area of Turin, as this area cannot be connected to the DHN because of technical constraints, which it is indicated in italic grey. The buildings with no production indicate the presence of constraints.

It is possible to observe that most of the buildings in Turin have a limited available roof area, that is, from 60 to 200 m$^2$. This area is even lower when excluding the hilly area, which becomes 25 to 200 m$^2$; these

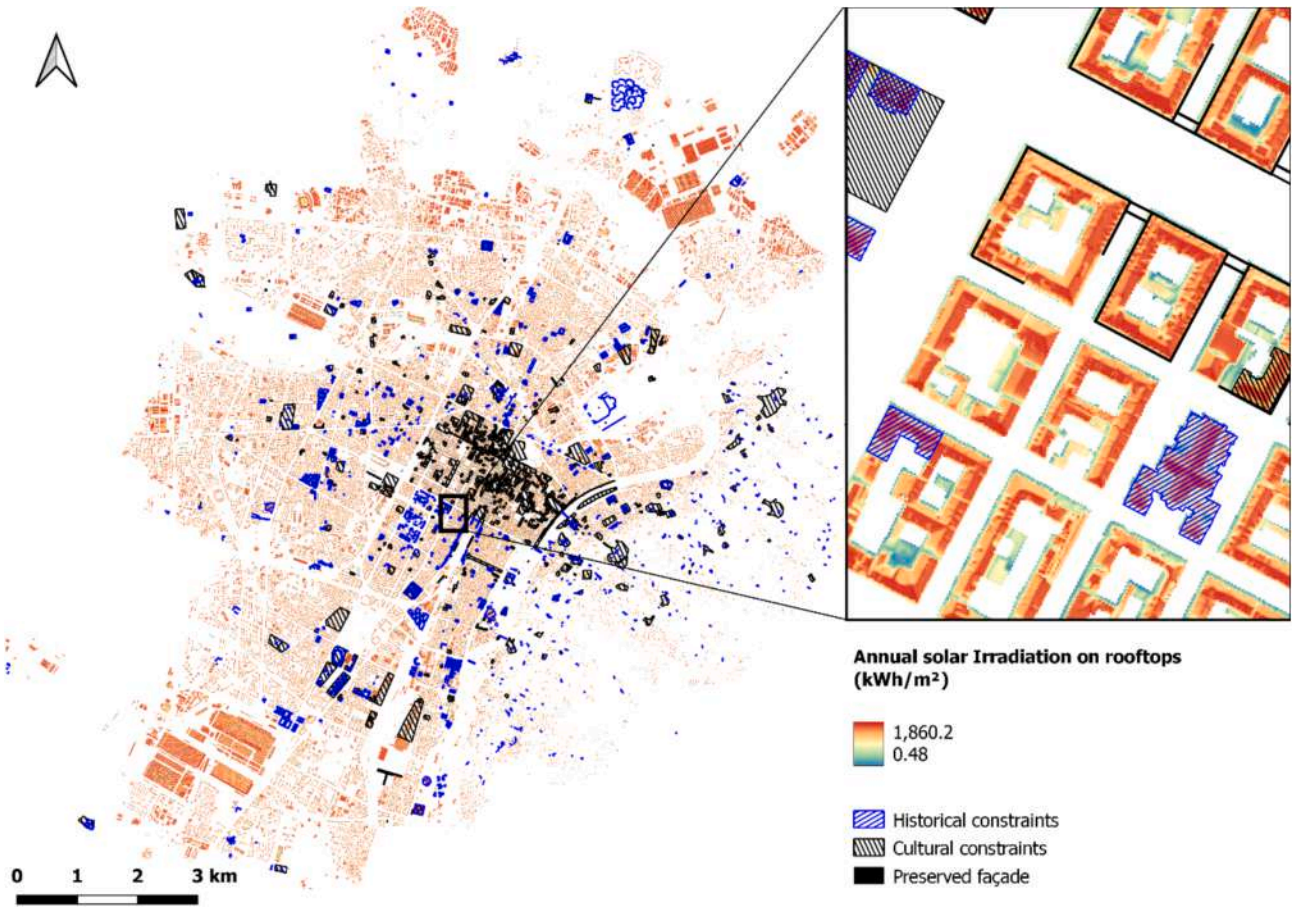


**Fig. 5.** Annual solar irradiation and the local constraints.

**Table 7**
Technical characteristics of the STC and PV.

| | STC | |
|---|---|---|
| | Flat plate | Vacuum Tube |
| $\eta_0$ | 0.855 | 0.70 |
| $a_1$ (W/m$^2$/K) | 2.41 | 1.15 |
| $a_2$ (W/m$^2$/K$^2$) | 0.039 | 0.011 |
| | **PV panels** | |
| | Monocrystalline silicon | |
| $\eta$ | 21.3 % | 23 % |

buildings are mainly condominiums, and there are skylights, dormers, chimneys and/or other objects on the roofs that hinder the installation of solar panels.

After segmenting the rooftops and excluding those unsuitable for installation, the number of buildings considered in this analysis decreased. Table 6 presents the total number of residential buildings available in Turin before and after the elimination process, which was based on physical, historical, and legal constraints. The table also provides the total available roof areas.

## 14. Solar irradiation results

Solar irradiation was simulated for each typical day using the *r.sun. insoltime* tool in QGIS. The results were compared with the irradiation data acquired from PVGIS online tool considering the 2006–2020 period. The results of QGIS simulations showed low errors when compared to PVGIS, if tailored horizon height profiles are provided as an input data to PVGIS, yielding an average annual error of 14 %, which is reflecting an acceptable value in this work considering the urban scale analysis performed.

The results of the annual solar irradiation are represented in Fig. 5, together with the cultural and historical constraints, to facilitate the understanding of their distribution throughout the city; areas where panel installation is not allowed are indicated. The historic center of Turin shows a high density of black outlines, which indicate the presence of restricted façades and roofs.

## 15. Energy production with solar technologies

The solar irradiation values of each roof segment were utilized to calculate the production of STC and PV using Eq. (2), Eq. (3) and Eq. 4. A flat plate collector and a vacuum tube collector were employed in this analysis. Detailed specifications, including optical efficiency ($\eta_0$), the heat loss coefficient ($a_1$), and the temperature dependence of the heat loss coefficient ($a_2$) are provided in Table 7. Moreover, two monocrystalline PV panels, with different efficiencies, were used for the electricity production scenarios.

The efficiency of the utilized panels was determined for each roof orientation on the basis of the irradiation quota of that particular orientation and the used panel technology. The efficiency was calculated for the three different energy services, that is, H, H + DHW, and DHW, using the inlet and outlet temperatures of the defined scenarios. Subsequently, the production was calculated using the daily efficiencies.

Fig. 6 shows the annual production for each roof orientation, with the south oriented roofs and flat roofs accounting for 70 % of the overall annual STC production. Calculating the production on different roof orientations helped to define the most feasible orientations for the installation of STC. Consequently, for the evaluated future scenarios,

| | South oriented roofs (%) |
|---|---|
| Residential | 32.4% |
| Mixed use residential | 29.5% |
| Commercial | 8.1% |
| Industrial | 18.8% |
| Educational | 3.4% |
| Health care | 1.4% |
| Other types of use | 4.8% |
| Not specified | 1.6% |

(a)

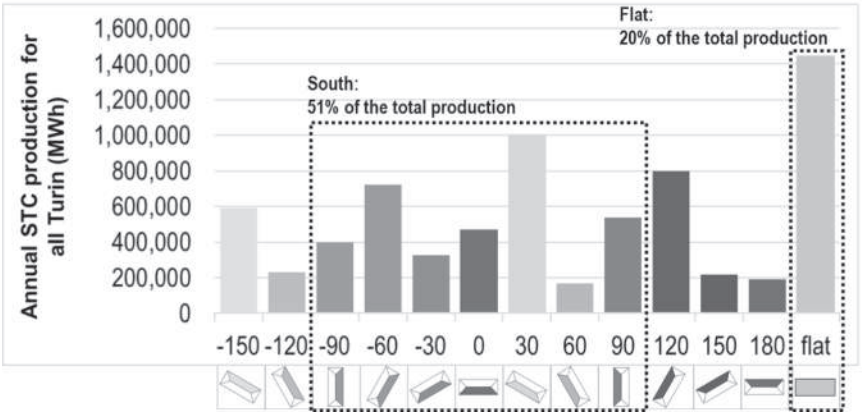


(b)

**Fig. 6.** Energy production percentages from different users (a) and annual STC production for H service (Scenario 2) using vacuum tube collector with 50–90 °C.

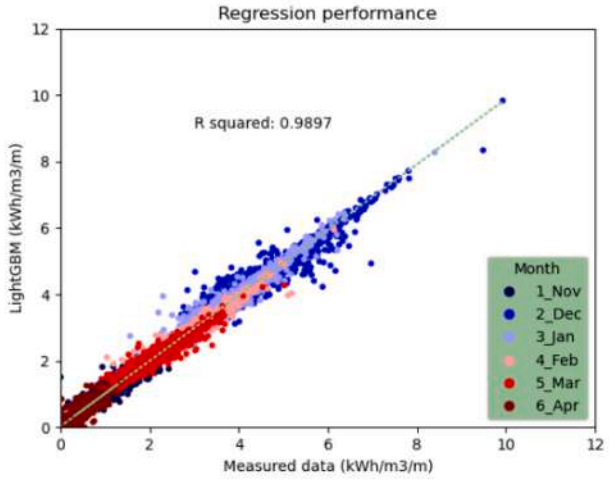


(a) H Prediction

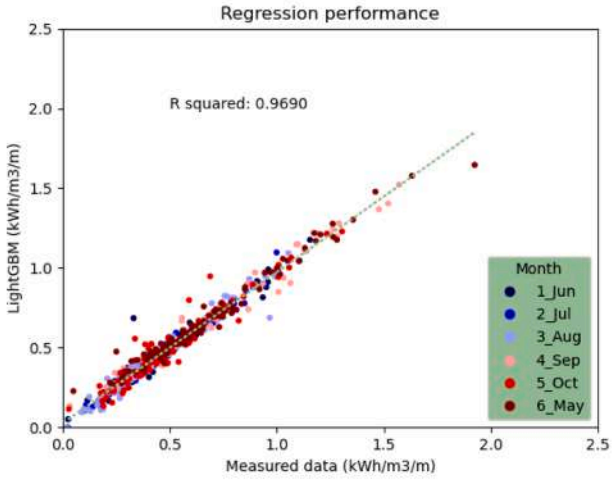


(b) DHW Prediction

**Fig. 7.** Energy consumption modeling (monthly) with LGBM.

only south orientated and flat roofs were considered.

It is necessary to analyze the production quota according to the type of building to identify the potential end-users that should be included in the collective consumption scenarios. The table on the left (Fig. 6a) shows that the highest production was generated from residential use, which was the main focus of this work.

## 16. Energy consumption modeling results

LGBM was used to predict the energy consumption of the two service types, H and DHW, considering all the residential buildings in Turin. Fig. 7 illustrates the accuracy of the monthly energy consumption prediction, that is, with $R^2$ 0.99 and 0.97, RMSE of 2.5 % and 3 % for H and DHW, respectively. This accuracy in prediction suggests that the results are sufficiently reliable to conduct further analysis of the STC potential to satisfy the energy demand of residential buildings.

Fig. 8 shows the importance of each different variable on the energy consumption modeling. The consumption of both energy services was generally mainly affected by the sky view factor (SVF), the surface-to-volume ration (S/V), and by climatic variables.

Finally, the annual consumption for the H, DHW, and E services considered in the analysis of this work are provided in Table 8 with:

- the number of buildings considered for each type of use,
- the annual consumption data related to the 2022–2023 period for H, DHW and E.

## 17. Self-consumption and self-sufficiency scenarios with an exergy analysis

The self-consumption index (SCI) and the self-sufficiency index (SSI) were computed using Eq. 5.2, focusing on flat and south-oriented roofs.

Table 9 summarizes the energetic results of this analysis by presenting the annual SCI, SSI, and OPI considering the nine scenarios. This analysis was instrumental in identifying the optimization methods that could be used to achieve a high energy share while reducing overproduction. Table 9 presents important insights into the influence of various energy services on the self-consumption levels. The utilization of all the available south-oriented roof surfaces and flat roofs inherently enhanced the self-sufficiency index (SSI), but it also led to a decrease in the self-consumption index (SCI) due to the high OPI. This can be explained by the negative load correlation between space heating and solar irradiation; a high space heating demand occurred during the lowest solar irradiation periods and vice-versa. Low values of self-consumption and self-sufficiency indexes can be observed in scenarios

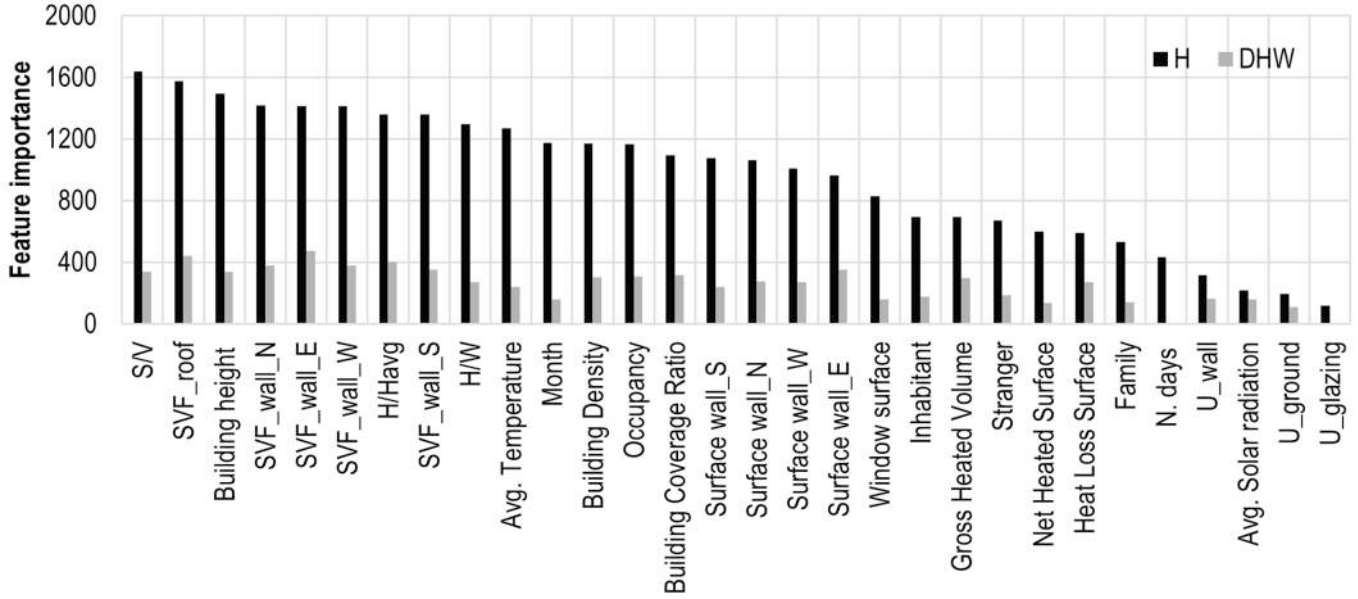


**Fig. 8.** The importance of the features of the different variables used in the energy consumption modeling.

**Table 8**
Annual consumption by the type of user.

| | Number of buildings (and block of buildings) | Annual H consumption [GWh] | Annual DHW consumption [GWh] | Annual E consumption [GWh] |
|---|---|---|---|---|
| Residential | 23,487 | 1063 | 504 | 468 |
| Mixed use residential | 12,743 | 1251 | 590 | 532 |
| Commercial | 2665 | 0.5 | Not calculated | Not calculated |
| Educational | 806 | 0.21 | 0.16 | Not calculated |
| Others | 3754 | Not calculated | Not calculated | Not calculated |

**Table 9**
Self-consumption scenarios for the different energy services.

| | Scenario N. | | Production (GWh) | Consumption (GWh) | SC (GWh) | SCI (%) | SSI (%) | OPI (%) |
|---|---|---|---|---|---|---|---|---|
| **Vacuum tube** | | | | | | | | |
| H (60–105 °C) | **1** | Energy | 2121 | 2314 | 181 | 8.54 % | 7.83 % | 91.46 % |
| | | Exergy | 407 | 592 | 43 | 10.45 % | 7.19 % | 89.55 % |
| H (50–90 °C) | **2** | Energy | 2347 | 2314 | 215 | 9.16 % | 9.29 % | 90.84 % |
| | | Exergy | 383 | 531 | 45 | 11.65 % | 8.40 % | 88.35 % |
| H (60–70 °C) | **3** | Energy | 2420 | 2314 | 227 | 9.36 % | 9.79 % | 90.64 % |
| | | Exergy | 367 | 531 | 45 | 12.32 % | 8.52 % | 87.68 % |
| H (50–60 °C) | **4** | Energy | 2485 | 2314 | 248 | 9.96 % | 10.70 % | 90.04 % |
| | | Exergy | 314 | 531 | 45 | 14.28 % | 8.44 % | 85.72 % |
| H (40–50 °C) | **5** | Energy | 2654 | 2314 | 275 | 10.37 % | 11.90 % | 89.63 % |
| | | Exergy | 264 | 531 | 44 | 16.62 % | 8.26 % | 83.38 % |
| H + DHW (40–50 °C) | **6** | Energy | 2654 | 3408 | 826 | 31.12 % | 24.24 % | 68.88 % |
| H (15.3–80 °C) | **7** | Energy | 2621 | 2314 | 271 | 10.35 % | 11.72 % | 89.65 % |
| DHW (15.3–48 °C) | **8** | Energy | 2942 | 1094 | 735 | 24.97 % | 67.16 % | 75.03 % |
| **Flat plate** | | | | | | | | |
| H (60–105 °C) | **1** | Energy | 1624 | 2314 | 95 | 5.85 % | 4.10 % | 94.15 % |
| | | Exergy | 308 | 592 | 23 | 7.45 % | 3.88 % | 92.55 % |
| H (50–90 °C) | **2** | Energy | 2086 | 2314 | 141 | 6.74 % | 6.08 % | 93.26 % |
| | | Exergy | 337 | 531 | 29 | 8.64 % | 5.48 % | 91.36 % |
| H (60–70 °C) | **3** | Energy | 2145 | 2314 | 154 | 7.16 % | 6.64 % | 92.84 % |
| | | Exergy | 322 | 531 | 31 | 9.59 % | 5.81 % | 90.41 % |
| H (50–60 °C) | **4** | Energy | 2502 | 2314 | 192 | 7.66 % | 8.28 % | 92.34 % |
| | | Exergy | 312 | 531 | 35 | 11.14 % | 6.54 % | 88.86 % |
| H (40–50 °C) | **5** | Energy | 2851 | 2314 | 236 | 8.27 % | 10.19 % | 91.71 % |
| | | Exergy | 279 | 531 | 38 | 13.75 % | 7.13 % | 86.43 % |
| H + DHW (40–50 °C) | **6** | Energy | 2851 | 3408 | 784 | 27.50 % | 23 % | 72.48 % |
| H (15.3–80 °C) | **7** | Energy | 2774 | 2314 | 226 | 8.13 % | 9.75 % | 91.87 % |
| DHW (15.3–48 °C) | **8** | Energy | 3452 | 1094 | 716 | 20.73 % | 65.40 % | 79.27 % |

| PV | Scenario N. | Production (GWh) | Consumption (GWh) | SC (GWh) | SCI (%) | SSI (%) | OPI (%) |
|---|---|---|---|---|---|---|---|
| E (η 21.3 %) | **9** | 814 | 1000 | 533 | 65.58 % | 53.37 % | 34.42 % |
| E (η 23 %) | | 878 | 1000 | 555 | 63.12 % | 55.47 % | 36.88 % |

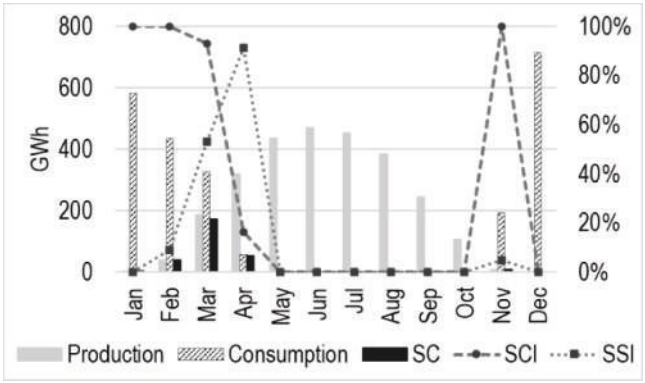


(a) Vacuum tube: scenario 5 H 40-50

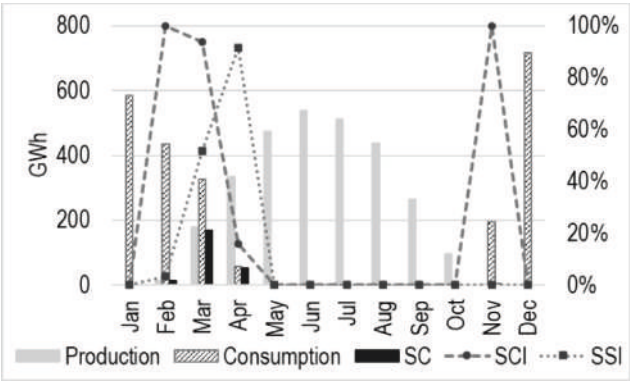


(d) Flat plate: scenario 5 H 40-50

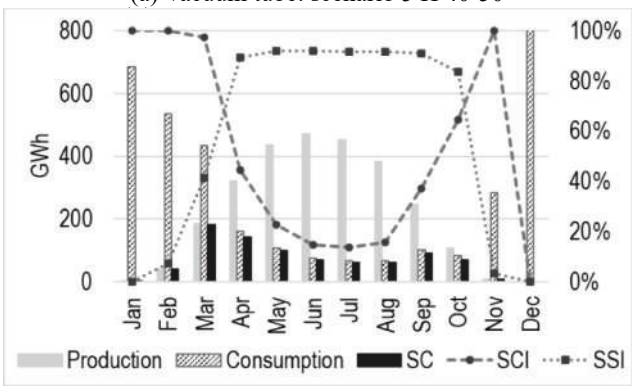


(b) Vacuum tube: scenario 6 H + DHW 40-50

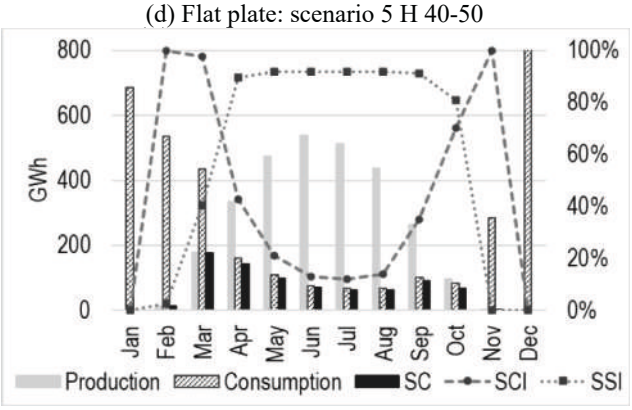


(e) Flat plate: scenario 6 H + DHW 40-50

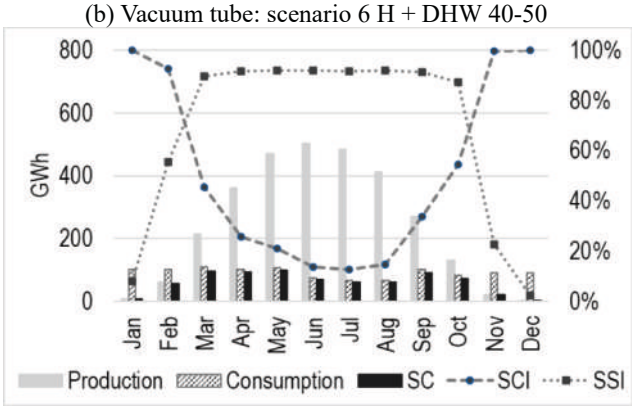


(c) Vacuum tube: scenario 8 DHW 15.6-48

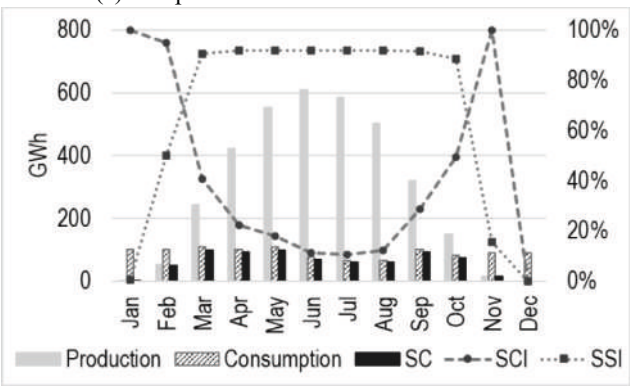


(f) Flat plate: scenario 8 DHW 15.6-48

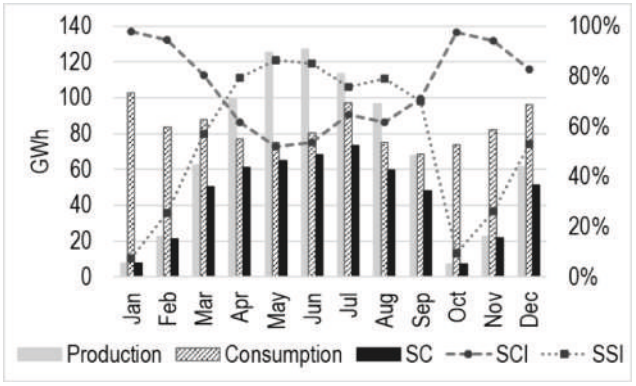


(g) PV monocrystalline η 21.3%: scenario 9

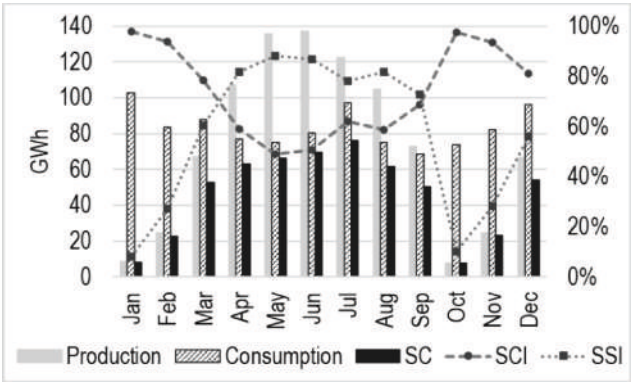


(h) PV monocrystalline η 23%: scenario 9

**Fig. 9.** Monthly production and consumption analysis of four service types: H on its own (a, d), H + DHW (b, e), DHW on its own (c, f), and E (g, h).

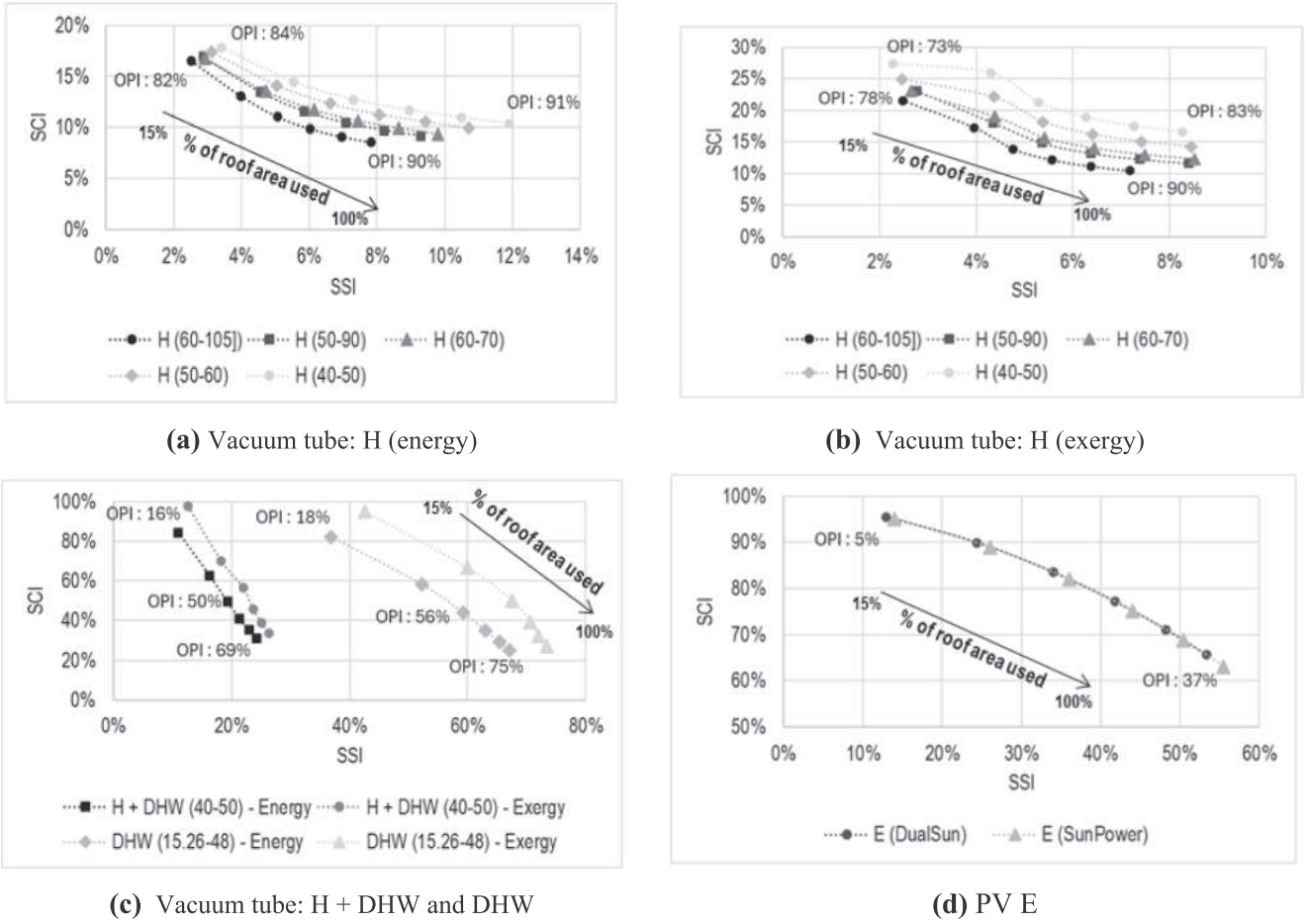


**(a)** Vacuum tube: H (energy)

**(b)** Vacuum tube: H (exergy)

**(c)** Vacuum tube: H + DHW and DHW

**(d)** PV E

**Fig. 10.** Energy index analysis of the different energy services: (a) Vacuum tube: H_energy, (b) Vacuum tube: H_exergy, (c) Vacuum tube: H + DHW and DHW_energy/exergy and (d) Monocrystalline PV panels.

with only H service (Scenarios 1 and 5); i.e., 4–12 % of SSI. Moreover, these indexes were obtained by over-sizing the solar systems with a very high over-production, that is, with an OPI of 89–94 %. A significant increase in self-consumed energy can be observed in the scenarios with the DHW service (Scenarios 6 and 8); i.e., from 12 % to 24—67 % of SSI with the vacuum tube collector.

All these scenarios assumed the full potential installation of STC across the available roof areas of the buildings, leading to a high annual OPI; these systems were over-sized, compared to the low energy demand in summer, and would not be technically or economically feasible without connection to the DHN. However, it is important to note that while the current analysis accounts for physical, regulatory, and legal constraints, it does not consider existing collectors, panels, or green roofs, as highlighted earlier. While incorporating these factors could slightly reduce overproduction, their overall impact is expected to be relatively minimal due to the limited presence of exiting solar technologies and green roofs in Turin.

The cells with the gray background in Table 9 show the results of the exergy analysis, in which the energy produced by STC at different temperatures was taken into account (Scenarios 1–5). Since exergy accounts for the quality of energy and its potential to perform useful work, this analysis provides deeper insights beyond the total energy produced and consumed. The correlation of the exergy with the mean thermodynamic temperature, $T_{m,}$ (Eq. 7) was used for this analysis as it offered higher accuracy. Similar SSI values can be observed for the different temperatures when comparing the use of STC for H service, ranging from 4 to 9 %.

PV panels for the electricity service show a higher potential than STC considering the self-consumption and self-sufficiency, with about 63 % and 55 %, respectively. The higher self-sufficiency, lower OPI and the possibility of injecting/selling energy to the grid suggests that this solar technology is more feasible than STC. These results are also presented with monthly SCI and SSI graphs in Fig. 9 for the various scenarios and solar technologies.

The monthly production and consumption data in Fig. 9 clearly show the high annual OPI values previously presented in Table 9, particularly for scenarios involving only the H service. One of the feasible solutions for these cases involves integrating different service types, such as DHW, which can utilize the surplus energy produced during summer. The monthly graphs also highlight that the vacuum tube collectors perform slightly better than flat plates in winter, and they even achieve a minimal production with the given temperatures in January, whereas flat plate collectors show almost no production in January and December.

Furthermore, both panels still show high OPI values in summer for the scenarios involving a mixed use (H + DHW), thus indicating that the DHW demand for residential buildings remains low because of the high energy production driven by high solar irradiation. This highlights the potential for integrating alternative end users, such as swimming pools or healthcare facilities, to better utilize the excess energy and increase the energy share.

Electricity consumption remains almost constant throughout the year, when considering the PV scenarios (Fig. 9 g and h), and this results in a lower OPI value than those of the STC, due to the higher proportion of self-consumed energy. As previously noted, the PV technology proved to be more practical and effective as a solar technology compared to STC, which is clearly illustrated in the monthly production and

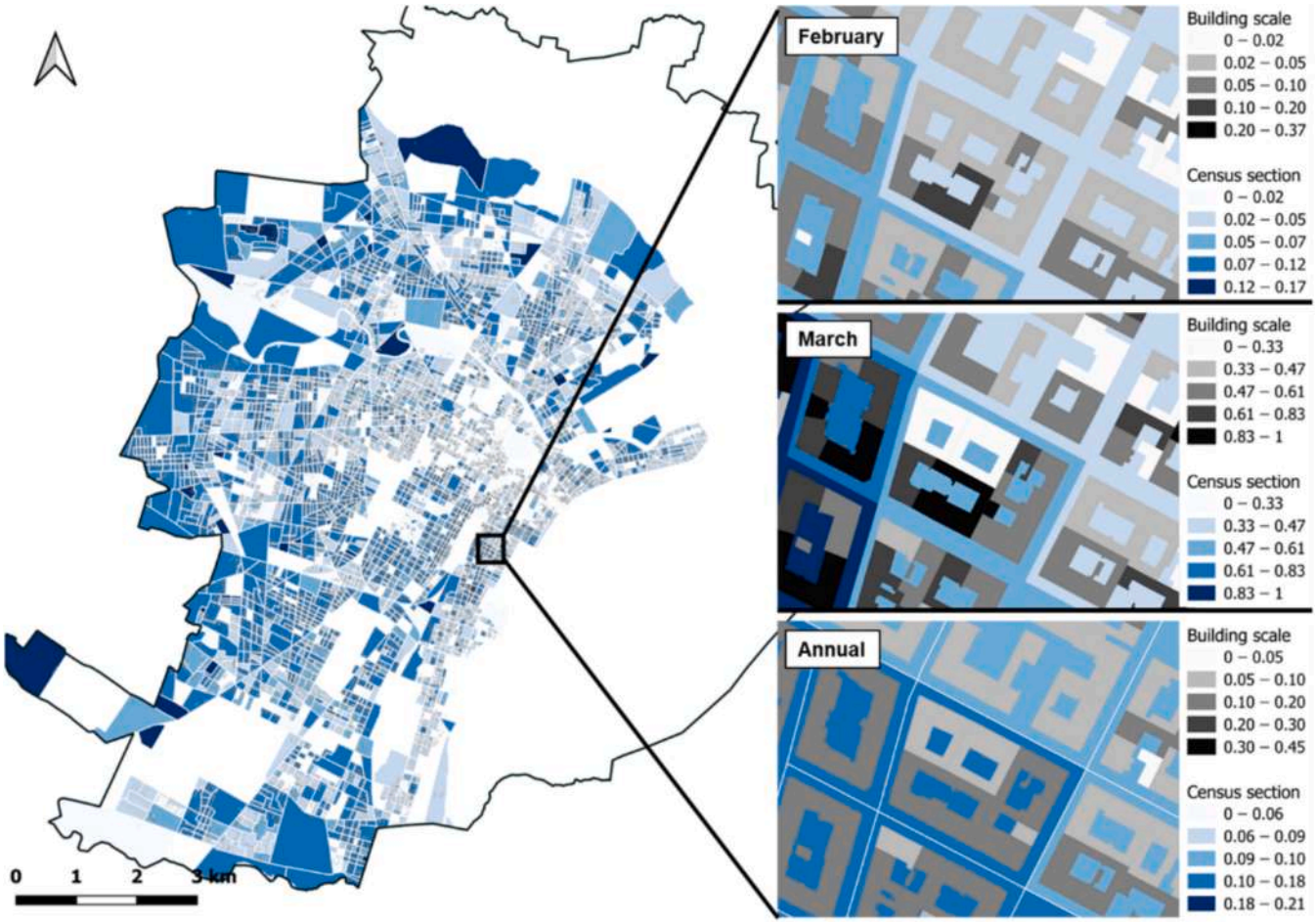


**Fig. 11.** Self-sufficiency for H service using vacuum tube collector with 50–90 °C.

consumption graphs.

Fig. 10 visualizes the results of the energy indexes for 6 different roof coverage percentages, for various energy services with PV and vacuum tube for STC. According to the results, the energy produced for the H service with lower outlet temperatures (Fig. 10a) yields a higher SSI for residential buildings, reaching 12 %, while the behavior of all temperature scenarios is relatively similar for the exergy (Fig. 10b). This is because the additional energy in the scenarios with lower temperatures is needed to increase the temperature of the flux that must be injected into the DHN. For this reason, exergy normalizes the energy to the maximum useful work that can be produced to make the various services comparable.

The high values of the OPI in scenarios with only H service are the result of a negative correlation between consumption and production. Since the high share of energy is produced in the summer, when the heating system is inactive, the produced energy is wasted.

Adding the DHW service to the DHN helps to harvest the wasted heat in the summer, and the SSI consequently rises from 10 % to nearly 30 %, moving from the H to the H + DHW services (Fig. 10c). Although the DHW service helps to increase the feasibility of the STC installation by increasing the SSI, but since the OPI reaches 70 % when all the available surfaces of south-oriented roofs are used (100 % roof coverage) for the

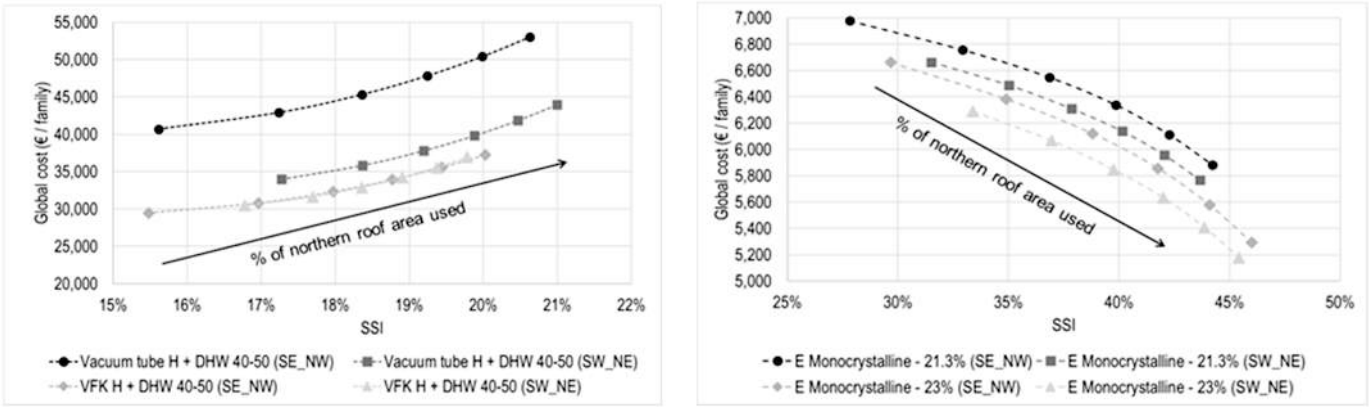


**Fig. 12.** Cost-optimal analysis of the PV scenarios in which solar panels are integrated for northern (NE_-150° or NW_+120°) orientations of the roof surfaces.

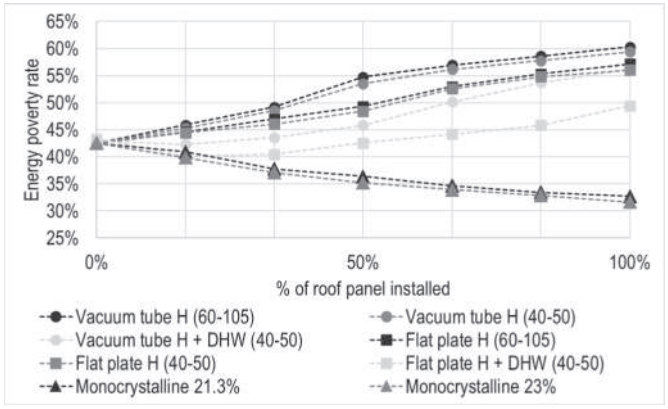


**(a)** Energy poverty without a tax deduction

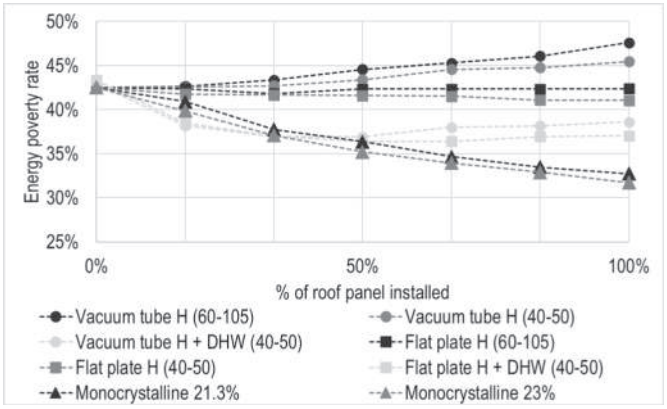


**(b)** Energy poverty with a 70% tax deduction (reduction on STC investment costs over 10 years)

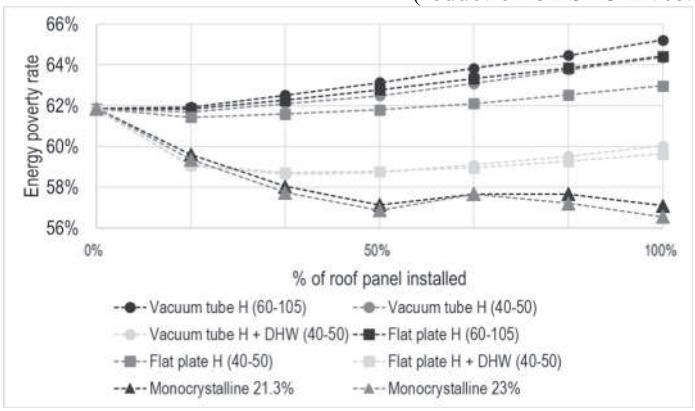


**(c)** Energy poverty in CAP zone 10156 with a 70% tax deduction

**Fig. 13.** The impact of integrating solar technologies in energy poverty.

installations, it is not an optimal solution for RES integration. PV systems show a more reliable performance, because installing PV makes it easier to reach a relatively high SSI of nearly 55 %, while the OPI value is less than 40 % as a maximum (Fig. 10d). This makes PV systems a powerful solution for roof integrated solar technology.

Fig. 11 illustrates a map of the annual SSI for the H service, considering the use of vacuum tube collector with 50–90 °C, for both building and census section scales. Zoomed-in maps provide a clearer understanding of the SSI variations across different seasons, February and March in particular, as well as the annual performance. March demonstrates a scenario in which high energy production occurs for a low energy demand, where self-sufficiency levels are able to reach 100 %. However, the annual SSI values are significantly lower, with maximum levels of 45 % and 21 % for the building and census section scales, respectively. This annual reduction is mainly due to the absence of production during January and December, combined with a high energy demand for space heating. Additionally, aggregating results at the census section scale shows a further decrease in SSI, compared to the building scale, as not all the buildings within each census section have a sufficient roof area for panel installation.

## 18. Energy, economic, and social analysis

This section evaluates scenarios from the economic and social points of view.

Fig. 12 shows the results of the cost optimal analysis when solar panels have been added to the North-oriented roof surfaces to enhance the energy efficiency of the buildings. Only scenario 6 was analyzed with H + DHW services (with a lower OPI) for STC. It is possible to observe that the presence of STC on the northern parts of the roofs is not convenient. Instead, integrating PV panels on the North-oriented roofs increases the SSI while the global cost drop, so it is certainly cost-optimal. Most panels installed on the NW (+120°) orientation are more effective than the panels on the NE (−150°) orientation of the roofs. Because there is a high quota of obstacles on the SE oriented roofs, although the NW surfaces of the roofs assist to a great extent in covering the energy needs that cannot be produced on the SE surfaces.

According to the Bernard Boardmann definition of energy poverty, households are in an energy poverty status if over 10 % of their annual disposable income is spent on energy services. The average annual income of the households in each Codice di Avviamento Postale (CAP) zone (Postal zone) was extracted from the Corriere website [34] to evaluate energy poverty at the building scale. This information was then distributed over the buildings in each zone to conduct a poverty evaluation of the buildings. The global cost of installing panels on all the available south-oriented roof surfaces was calculated using Eq. 8 for various solar technology scenarios. The calculation of the global cost was based on the assumptions made for the socioeconomic analysis, which are mentioned in the Materials and Methods section. The buildings that were considered to be at risk of energy poverty were calculated by comparing the global cost, normalized by the number of families and 10 % of the annual income per family, and the results are visualized in Figs. 13 and 14.

The energy poverty status of the entire city of Turin is shown in Fig. 13 a and b for all the scenarios, considering two assumptions:

- First, the analysis was conducted without incentives on the installation of solar technologies. The only benefit taken into account was “Social Bonus 2024” on the energy bills for low-income families.

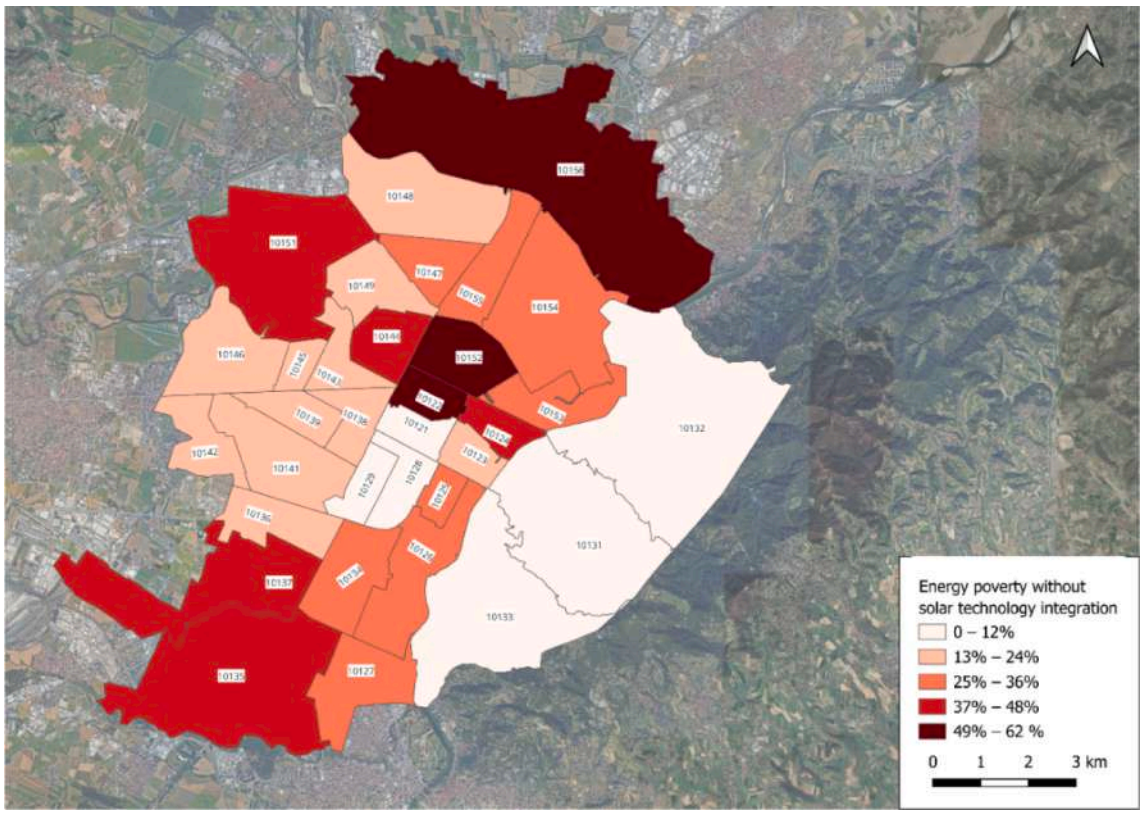


**(a)** Energy poverty before installing solar technologies

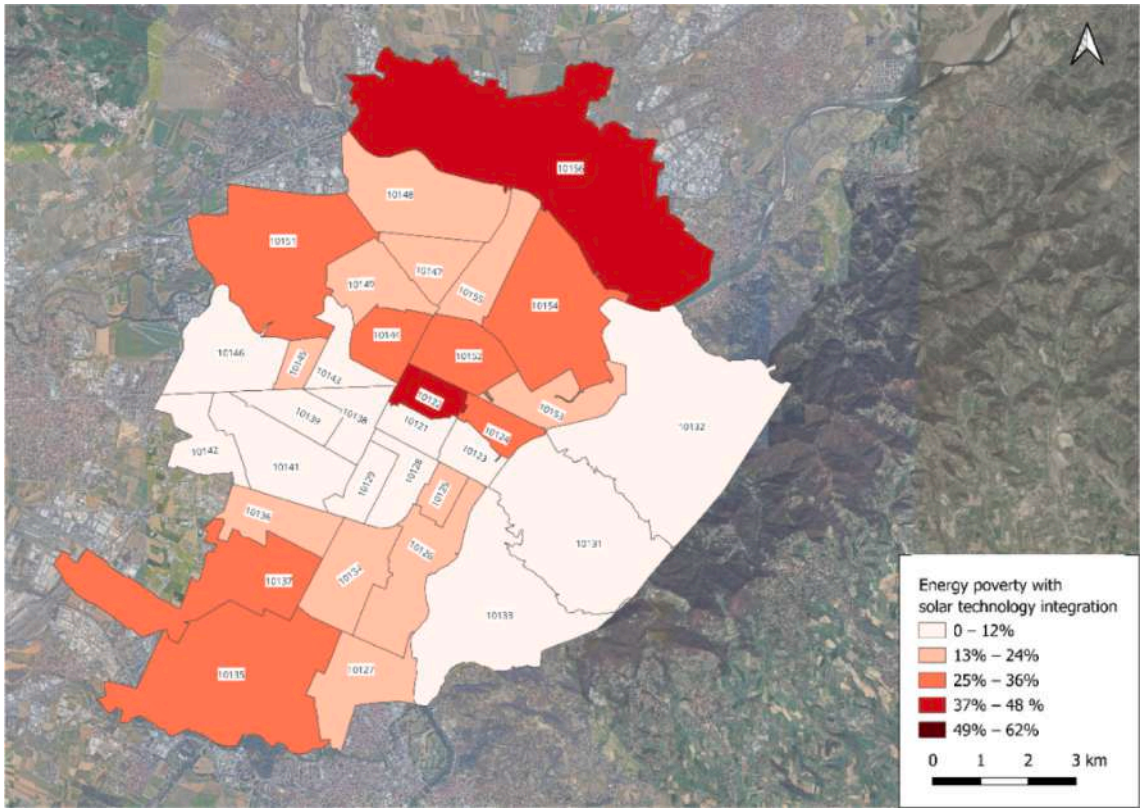


**(b)** Energy poverty after installing PV on 50% of the available roofs and STC on 50% of the available roofs and with a 70% tax deduction incentive

**Fig. 14.** The energy poverty status in Turin before and after integrating solar technologies.

- Secondly, the analysis considered a tax deduction of 70 % on the cost of STC.

According to the results, PV panel installation is beneficial in reducing energy poverty by 10 %; consequently, without dedicating any incentives to PV panels, they are still economically beneficial for vulnerable households. On the other hand, STC without incentives has no effect on reducing energy poverty, although it becomes influential with 70 % of incentives.

It was found, for the H + DHW scenario, that installing STC on 50 % of the available surfaces of south-oriented roofs helped to reduce energy poverty by about 6 %. This was found to be the best ratio to install STC, since, over this share of STC integration, the energy poverty starts to increase. Consequently, a good possible scenario to avoid energy poverty could involve the integration of STC on 50 % of the surfaces on the south-oriented roofs, while the remaining part could be used for PV installation. Energy poverty was further examined for CAP zone 10156, which has the highest EPI, as can be seen in Fig. 13c. It is possible to observe that Scenario 6 for H + DHW 40–50 °C is convenient for up to 50 % of the roof area, while Scenario 5 for H 40–50 °C is convenient for up to 15 %.

The maps in Fig. 14 a and b show the status of energy poverty for the current and after solar technology integration respectively, focusing on the optimal solution introduced above. According to the maps, the households in the city center and hills are more energy secure, while a high share of families living in CAP zones 10156, 10152, and 10,122 suffer from high energy poverty (Fig. 14a). After the installation of solar technologies (Fig. 14b), the reduction in energy costs helped to reduce the energy poverty risk in almost every neighborhood in the city, in particular the highly vulnerable areas mentioned above, but also in other areas, such as CAP zone 10144, which underwent a reduction of 40 % of the EPI (calculated using Eq. 5.2).

## 19. Conclusion

The aim of the presented work was to introduce a novel approach to the integration of solar technologies in dense urban environment. The primary contribution of this work was the development of an urban-scale roof assessment methodology, which accounted for physical, regulatory, and legal constraints, enabling a precise identification of areas suitable for the installation of solar technologies.

The methodology was applied to analyze the potential integration of STC in the city of Turin using a place-based approach with Urban Building Energy Modeling (UBEM) and to compare its potential with the PV technology. By employing a detailed roof analysis, this work not only examined the available areas for the installation of STC and PV but also excluded constraints like dormer windows and historical or cultural restrictions. The energy performance of STC was evaluated using different inlet and outlet water temperatures and considering different indicators and indexes to measure the impact of this technology. The aim has also been to evaluate the most suitable solution to improve the share of renewables in the DHN.

The analysis revealed that the use of solar technologies mainly depends on the energy service. The self-sufficiency with STC was found to be low for space heating (H), and it was influenced to a great extent by the low solar irradiation in the colder months and thus by the higher supply temperature that was needed. The self-sufficiency increased for domestic hot water (DHW) and electricity (E) because of the constant energy demand over all the seasons, together with the lower operating temperatures of STC. Twelve percent of SSI can be reached for H when all the roofs of the residential buildings are used, with an OPI of 91 %, which is so high and limits the economic convenience of this intervention. It emerged, from the exergy analysis, that the STC with different temperatures showed similar low SSI. The self-sufficiency reached 24 % for H + DHW, with an over-production of 69 %; the SSI was about 67 % for DHW on its own, with an over-production of 79 %. The best results were obtained for E with PV, which showed an SSI of 55 % and 37 % of over-production.

A cost-benefit analysis was then conducted considering solutions with different roof orientations. However, the findings of the cost optimal analysis showed that the installation of STC could be a challenge for DHW and H + DHW services with incentives. They might be beneficial for use at a building scale, but not at the district/urban scale; they were more feasible for PV panels, and all the solutions were found to be cost effective.

As far as the social impact of solar technologies is concerned, the energy poverty index was evaluated after the installation of STC (50 % for H + DHW) and PV (50 % for E) for the different neighborhoods in Turin. A reduction of EPI of 20–40 % was observed.

The methodology presented in this study offers valuable insights into the feasibility of utilizing solar technologies in urban settings. The presented methodology provides a flexible approach that can be applied to different urban contexts using available open-source tool, i.e., QGIS, and available geo-databases. This approach can respond to the needs of various stakeholders, including policymakers, urban planners, and citizens, to assess the potential of the adoption of renewable energy and to address environmental constraints in urban environments.

## CRediT authorship contribution statement

**Y. Usta:** Writing – review & editing, Writing – original draft, Software, Methodology, Formal analysis, Data curation. **A. Montazeri:** Writing – review & editing, Writing – original draft, Software, Methodology, Formal analysis, Data curation. **G. Mutani:** Writing – review & editing, Writing – original draft, Supervision, Resources, Methodology, Funding acquisition, Data curation, Conceptualization.

## Declaration of competing interest

The authors declare the following financial interests/personal relationships which may be considered as potential competing interests: Ahad Montazeri reports financial support was provided by Ministero dell'università e della ricerca. Guglielmina Mutani reports financial support was provided by IREN. If there are other authors, they declare that they have no known competing financial interests or personal relationships that could have appeared to influence the work reported in this paper.

## Acknowledgments

This work is part of the "Green District Heating GDH" research project, which involves a joint working group between the Politecnico di Torino and IREN (the district heating company in Turin). It was developed with the aim of identifying the methods and technologies necessary for the energy transition of the DHN in Turin, coordinated by Prof. Vittorio Verda of the Politecnico di Torino. This publication is part of the PNRR-NGEU project which has received funding from the MUR–DM118/2023.

## Data availability

Data will be made available on request.

## References

[1] United Nations, World Urbanization Prospects – 2018 Revision. https://population.un.org/wup/, 2018 (accessed 20 November 2024).
[2] European Commission, Renewable Energy Directive – REDIII. https://energy.ec.europa.eu/topics/renewable-energy/renewable-energy-directive-targets-and-rules/renewable-energy-directive_en, 2023 (accessed 20 November 2024).
[3] United Nations, The Paris Agreement. https://www.un.org/en/climatechange/paris-agreement, 2015 (accessed 20 November 2024).
[4] European Parliament, Circular economy: definition, importance and benefits. https://www.europarl.europa.eu/topics/en/article/20151201STO05603/circula

r-economy-definition-importance-and-benefits, 2014 (accessed 20 November 2024).
[5] Eurostat, News Release – 2023. https://ec.europa.eu/eurostat/web/products-eurostat-news/w/ddn-20230130-1, 2023 (accessed 20 November 2024).
[6] E. Lucchi, S. Baiani, P. Altamura, Design criteria for the integration of active solar technologies in the historic built environment: taxonomy of international recommendations, Energ. Buildings 278 (2023) 112651, https://doi.org/10.1016/j.enbuild.2022.112651.
[7] Energy Agency (IEA), Solar Heat Worldwide. https://www.iea-shc.org/solar-heat-worldwide, 2023 (accessed 20 November 2024).
[8] International Energy Agency (IEA), Renewables Report – 2021. https://www.iea.org/reports/renewables-2021, 2021 (accessed 20 November 2024).
[9] L.J. Houchmand, M. Macarulla Martí, S. Gassó-Domingo, Photovoltaics and green roofs: Holistic analysis in built environments, Renew. Sustain. Energy Rev. 207 (2025) 114987, https://doi.org/10.1016/j.rser.2024.114987.
[10] International Energy Agency (IEA), Net Zero Emissions by 2050 Scenario (NZE). https://www.iea.org/reports/global-energy-and-climate-model/net-zero-emissions-by-2050-scenario-nze (accessed 20 November 2024).
[11] International Energy Agency (IEA), Energy Systems: District Heating – 2023 Report. https://www.iea.org/reports/tracking-clean-energy-progress-2023, 2023 (accessed 20 November 2024).
[12] K. Lebedeva, L. Migla, T. Odineca, Solar district heating system in Latvia: A case study, J. King Saud Univ. Sci. 35 (2023) 102965, https://doi.org/10.1016/j.jksus.2023.102965.
[13] M. Bilardo, J. Kämpf, E. Fabrizio, Energy assessment of a district by integrating solar thermal in district heating network: a dynamic analysis approach, J. Phys. Conf. Ser. 2600 (2023) 052005, https://doi.org/10.1088/1742-6596/2600/5/052005.
[14] J. Solano, M. Frossard, S. Lasvaux, et al., Life cycle assessment of the new solar thermal power plant SolarCAD II connected to a District Heating Network in Geneva, Switzerland, J. Phys.: Conf. Series 2600 (2023) 152005, https://doi.org/10.1088/1742-6596/2600/15/152005.
[15] S. Selvakkumaran, L. Axelsson, I.-L. Svensson, Drivers and barriers for prosumer integration in the Swedish district heating sector, Energy Rep. 7 (2021) 193–202, https://doi.org/10.1016/j.egyr.2021.10.001.
[16] Y. Zhang, D. Wang, G. Wang, P. Xu, Y. Zhu, Data-driven building load prediction and large language models: comprehensive overview, Energ. Buildings 326 (2025) 115001, https://doi.org/10.1016/j.enbuild.2024.115001.
[17] K.Z. Dadjiogou, A.S.A. Ajavon, Y. Bokovi, Energy flow management in a smart microgrid based on photovoltaic energy supplying multiple loads, J. Sustainable Develop. Energy Water Environ. Syst. 12 (1) (2024) 1110473, https://doi.org/10.13044/j.sdewes.d11.0473.
[18] Y. Usta, G. Carioni, G. Mutani, Mapping solar energy production with photovoltaic panels on Politecnico di Torino university campus, Energ. Effi. 17 (5) (2024) 53, https://doi.org/10.1007/s12053-024-10233-w.
[19] G. Mutani, V. Todeschi, Optimization of costs and self-sufficiency for roof integrated photovoltaic technologies on residential buildings, Energies 14 (13) (2021) 4018, https://doi.org/10.3390/en14134018.
[20] Geoportale Piemonte, BDTRE. https://www.geoportale.piemonte.it/geonetwork/srv/ita/catalog.search#/search?any=BDTRE, 2023 (accessed 20 November 2024).
[21] Geoportale Piemonte, Vincoli e prescrizioni sovraordinate - Beni culturali - Art. 10 D.Lgs 42/2004. https://www.geoportale.piemonte.it/geonetwork/auth/api/records/c_l219:0e13845a-000d-4e8b-9c64-c465f345401e, 2023 (accessed 20 November 2024).
[22] ENEA, Solaritaly | Values of Solar Radiation in Italy. http://www.solaritaly.enea.it/TabelleRad/TabelleRadEn.php, 2023 (accessed 20 November 2024).
[23] Meteonorm, Meteonorm Tool. https://meteonorm.com/en/, 2023 (accessed 20 September 2024).
[24] J.A. Duffie, W.A. Beckman, Solar Engineering of Thermal Processes, Wiley, 1991.
[25] ISTAT, Residential population in 2024. http://dati.istat.it/index.aspx?datasetcode=dcis_popres1, 2024 (accessed 20 November 2024).
[26] ARERA, Monthly electrical energy consumption. https://www.arera.it/dati-e-statistiche/dettaglio/analisi-dei-consumi-dei-clienti-domestici, 2023 (accessed 17 October 2024).
[27] C. Ma, C. Yuan, Y. Zhang, H. Hu, Mapping utilizable rooftop areas to meet food security goal in four high-density cities: a deep learning and GIS integrated approach, Sustainable Cit. Soc. 55 (2024) 106066, https://doi.org/10.1016/j.scs.2024.106066.
[28] G. Mutani, M. Alehasin, Y. Usta, F. Fiermonte, A. Marino, Statistical building energy model from data collection, place-based assessment to sustainable scenarios for the city of Milan, Sustainability 15 (20) (2023) 14921, https://doi.org/10.3390/su152014921.
[29] F. Spertino, F. Corona, Monitoring and checking of performance in photovoltaic plants: A tool for design, installation and maintenance of grid-connected systems, Renewable Energy 60 (2013) 722–732, https://doi.org/10.1016/j.renene.2013.06.011.
[30] European Parliament and Council, Directive (EU) 2023/1791 of 13 September 2023 on energy efficiency and amending Regulation (EU) 2023/955 (recast), Available from: https://eur-lex.europa.eu/eli/dir/2023/1791/oj/eng (accessed 28 January 2025).
[31] R. Volpe, E. Cutore, A. Fichera, Design and operational indicators to foster the transition of existing renewable energy communities towards positive energy districts, J. Sustainable Develop. Energy Water Environ. Syst. 12 (2) (2024) 1120513, https://doi.org/10.13044/j.sdewes.d12.0513.
[32] G. Evola, L. Marletta, Exergy and thermoeconomic optimization of a water-cooled glazed hybrid photovoltaic/thermal (PVT) collector, Sol. Energy 107 (2014) 12–25, https://doi.org/10.1016/j.solener.2014.05.041.
[33] C. Delmastro, G. Mutani, S.P. Corgnati, A supporting method for selecting cost-optimal energy retrofit policies for residential buildings at the urban scale, Energy Policy 99 (2016) 42–56, https://doi.org/10.1016/j.enpol.2016.09.051.
[34] Corriere della Sera, Average annual income of households. https://www.corriere.it/tecnologia-/23_luglio_18/redditi-torino-cap-quartiere-4d6299e3-d70d-473d-8a00-31b32db08xlk.shtml, 2023 (accessed 20 november 2024).
[35] ARERA, Bonus sociale per disagio economico: a quanto ammontano, Available from: https://www.arera.it/consumatori/bonus-sociale/bonus-sociale-per-disagio-economico/a-quanto-ammontano (accessed 28 January 2025).
[36] IREN Group, La rete di teleriscaldamento. https://www.gruppoiren.it/it/i-nostri-servizi/teleriscaldamento/la-nostra-rete.html, 2023 (accessed 10 September 2024).